THE JOURNAL OF BIOLOGICAL CHEMISTRY VOL. 289, NO. 23, pp. 16374–16388, June 6, 2014

Myeloid Cell-specific Disruption of *Period1* and *Period2* Exacerbates Diet-induced Inflammation and Insulin Resistance*

Received for publication, December 3, 2013, and in revised form, April 21, 2014 Published, JBC Papers in Press, April 25, 2014, DOI 10.1074/jbc.M113.539601

Hang Xu[‡1], Honggui Li[‡1], Shih-Lung Woo[‡1], Sam-Moon Kim[§], Vikram R. Shende[§], Nichole Neuendorff[§], Xin Guo[‡], Ting Guo[‡], Ting Qi[‡], Ya Pei[‡], Yan Zhao[‡], Xiang Hu[‡¶], Jiajia Zhao[‡‖], Lili Chen[‖], Lulu Chen[¶], Jun-Yuan Ji[**], Robert C. Alaniz[‡‡], David J. Earnest[§2], and Chaodong Wu[‡3]

From the [‡]Department of Nutrition and Food Science, Texas A&M University, College Station, Texas 77843, [§]Department of Neuroscience and Experimental Therapeutics, College of Medicine, Texas A&M Health Science Center, Bryan, Texas 77807, [¶]Department of Endocrinology and [‖]Department of Stomatology, Union Hospital, Tongji College of Medicine, Huazhong University of Science and Technology, Wuhan, Hubei 430022, China, and [**]Department of Molecular and Cellular Medicine and [‡‡]Department of Microbial and Molecular Pathogenesis, College of Medicine, Texas A&M Health Science Center, College Station, Texas 77843

Background: Circadian clockworks gate macrophage inflammatory responses.
Results: Myeloid cell-specific disruption of *Period1* and *Period2* exacerbates diet-induced adipose and liver inflammation and systemic insulin resistance.
Conclusion: Macrophage circadian dysregulation contributes to diet-induced inflammation and metabolic phenotypes in adipose and liver tissues.
Significance: Interactions between circadian clocks and pathways mediating adipose tissue inflammation are critical in the development and possibly treatment of obesity-associated metabolic disorders.

The circadian clockworks gate macrophage inflammatory responses. Given the association between clock dysregulation and metabolic disorders, we conducted experiments to determine the extent to which over-nutrition modulates macrophage clock function and whether macrophage circadian dysregulation is a key factor linking over-nutrition to macrophage proinflammatory activation, adipose tissue inflammation, and systemic insulin resistance. Our results demonstrate that 1) macrophages from high fat diet-fed mice are marked by dysregulation of the molecular clockworks in conjunction with increased proinflammatory activation, 2) global disruption of the clock genes *Period1* (*Per1*) and *Per2* recapitulates this amplified macrophage proinflammatory activation, 3) adoptive transfer of *Per1/2*-disrupted bone marrow cells into wild-type mice potentiates high fat diet-induced adipose and liver tissue inflammation and systemic insulin resistance, and 4) *Per1/2*-disrupted macrophages similarly exacerbate inflammatory responses and decrease insulin sensitivity in co-cultured adipocytes *in vitro*. Furthermore, PPARγ levels are decreased in *Per1/2*-disrupted macrophages and PPARγ2 overexpression ameliorates *Per1/2* disruption-associated macrophage proinflammatory activation, suggesting that this transcription factor may link the molecular clockworks to signaling pathways regulating macrophage polarization. Thus, macrophage circadian clock dysregulation is a key process in the physiological cascade by which diet-induced obesity triggers macrophage proinflammatory activation, adipose tissue inflammation, and insulin resistance.

Obesity is highly associated with systemic insulin resistance and the consequential development of a wide variety of metabolic diseases including type 2 diabetes (1), fatty liver disease (2), and cardiovascular disease (3). Over the past decade, adipose tissue inflammation has been increasingly regarded as a causal factor of obesity-associated insulin resistance (4–8). As demonstrated in mice fed a high fat diet (HFD),[4] adipose tissue develops low grade inflammation that is characterized by increased infiltration of immune cells and production of proinflammatory cytokines (4, 5). The diet-induced proinflammatory signaling coupled with increased production of pro-hyperglycemic factors (*e.g.* free fatty acids and resistin) and decreased production of anti-hyperglycemic factors (*e.g.* adiponectin) that reflect inflammation-associated adipose tissue dysfunction (9–12) collectively impair insulin signaling in insulin-sensitive

* This work was supported, in whole or in part, by National Institutes of Health Grants 1R01DK095828 and 1R01DK095862) (NIDDK; to C. W.). This work was also supported, in whole or in part, by American Diabetes Association Grants 1-10-JF-54 and 1-13-BS-214-BR, American Heart Association Grant 12BGIA9050003 (to C. W.).
[1] These authors contributed equally to this work.
[2] To whom correspondence may be addressed: Texas A&M Health Science Center, 8447 State Highway 47, Bryan, TX 77807. Fax: 979-436-0086; E-mail: DEARNEST@medicine.tamhsc.edu.
[3] To whom correspondence may be addressed: Texas A&M University, 2253 TAMU, College Station, TX 77843. Fax: 979-862-7782; E-mail: cdwu@tamu.edu.

[4] The abbreviations used are: HFD, high-fat diet; PPAR, peroxisome proliferator-activated receptor; TLR4, Toll-like receptor 4; Per, Period; Luc, luciferase; LFD, low-fat diet; BMT, bone marrow transplantation; BMDM, bone marrow-derived macrophage(s); SVC, stromal vascular cell(s); NF-κB, nuclear factor κB; MCP1, monocyte chemoattractant protein 1; SREBP1c, sterol regulatory element-binding protein 1c; FAS, fatty acid synthase; BMAL1, brain muscle ARNT-like protein 1; CLOCK, circadian locomotor output cycles kaput.

tissues including the liver and skeletal muscle, leading to systemic insulin resistance (13–18). In contrast, treatment with thiazolidinediones or supplementation with fish oils ameliorates adipose tissue inflammation, which in turn contributes to the reversal of diet-induced adipose tissue dysfunction and systemic insulin resistance (19–21). As such, obesity-associated inflammation is key to the regulation of systemic insulin sensitivity.

In relation to the link between inflammation and metabolic dysregulation in obesity, there is increasing evidence that dysregulated macrophage functional plasticity and versatility (polarization) is a key component of the mechanism by which inflammation in adipose and liver tissues mediates the development of obesity-associated insulin resistance and metabolic diseases. For example, in diet-induced obesity, adipose tissue macrophage infiltration is increased, and polarization is shifted toward the proinflammatory M1 activation, resulting in increased production of proinflammatory cytokines and potentiation of adipose tissue inflammation that contribute to impaired systemic insulin sensitivity (22). Within macrophages, peroxisome proliferator-activated receptor γ and δ (PPARγ/δ) are key transcription factors that stimulate macrophage alternative M2 (anti-inflammatory) activation (23–25). Importantly, myeloid cell-specific disruption of PPARγ and/or PPARδ increases proinflammatory activation of adipose tissue macrophages and exacerbates obesity-associated insulin resistance (6, 23). In contrast, the effect of PPARγ activation on reversing HFD-induced insulin resistance is mediated at least in part by stimulation of alternative activation of macrophages in adipose tissue (20). Macrophage polarization is also regulated by Toll-like receptor 4 (TLR4) and/or c-Jun N-terminal kinase (JNK) such that their myeloid cell-specific disruption protects mice from diet-induced adipose tissue inflammation and systemic insulin resistance (26–28). As such, these findings demonstrate how the inflammatory status of macrophages governs the outcome of adipose tissue inflammation and systemic insulin sensitivity.

Circadian clocks in peripheral tissues and cells drive daily rhythms and coordinate many physiological processes including inflammation and metabolism. Recent observations suggest that circadian clock dysregulation plays a key role in the development of metabolic diseases including obesity and diabetes. Studies using mice with genetic mutation or deletion of core clock genes correspondingly indicate that global and adipocyte-specific disruption of circadian clock function produces obesity or significant alterations in metabolism (29–31). However, the specific mechanism underlying the link between circadian clock- and metabolic-dysregulated phenotypes is unknown. As key components of inflammation in obesity, macrophages contain cell-autonomous circadian clocks that have been shown to gate macrophage inflammatory responses including rhythms in lipopolysaccharide (LPS)-induced cytokine secretion (32, 33). Because HFD induces adipose tissue circadian clock dysregulation in conjunction with adipose tissue macrophage proinflammatory activation (34) and environment-mediated circadian disruption amplifies macrophage proinflammatory responses (35), our hypothesis is that over-nutrition causes circadian clock dysregulation, which in turn induces macrophage proinflammatory activation in adipose tissue so as to exacerbate inflammation and fat deposition, thus leading to systemic insulin resistance. To test this hypothesis, we conducted a series of experiments to determine whether 1) HFD induces circadian clock dysregulation along with proinflammatory activation in indigenous and adipose tissue macrophages, 2) genetic disruption of the clock mechanism using mice with targeted mutations of the clock genes *Period1* (*Per1*) and *Per2* ($Per1^{ldc}$/$Per2^{ldc}$) alters macrophage proinflammatory status, 3) PPARγ plays a role in the proinflammatory activation of *Per1*/*2*-disrupted macrophages, and 4) adoptive transfer or co-culture of *Per1*/*2*-disrupted macrophages potentiates inflammatory responses and pathophysiology of adipose tissue in diet-induced obesity or adipocytes *in vitro*.

EXPERIMENTAL PROCEDURES

Animal Experiments—Animals used in this study were derived from wild-type (WT) C57BL/6J mice and 129J mice obtained from The Jackson Laboratory (Bar Harbor, ME) and from breeding pairs of homozygous $mPer2^{Luc}$ knockin mice (C57BL/6J background; generously provided by Dr. Joseph Takahashi, UT Southwestern Medical School, Dallas, TX) and homozygous mutant mice with targeted disruption of the clock genes, *Per1* and *Per2* ($Per1^{ldc}$/$Per2^{ldc}$; generously provided by Dr. David Weaver, University of Massachusetts Medical School, Worcester, MA). In homozygous $mPer2^{Luc}$ mice, a luciferase (Luc) gene was fused in-frame to the C terminus of the endogenous mPER2 coding sequence so as to enable continuous recording of *Per2* oscillations via luciferase bioluminescence (36). Establishment, genotyping, and phenotype of $Per1^{ldc}$/$Per2^{ldc}$ mutant mice (129J background) have been described previously (37). $Per1^{ldc}$/$Per2^{ldc}$ mice are distinguished by a loss of circadian rhythmicity as well as altered expression and circadian regulation of other clock genes (37). In different peripheral tissues, $Per1^{ldc}$/$Per2^{ldc}$ mutant mice consistently showed increased BMAL1 (~600%) and increased CLOCK (~65%) protein levels relative to WT controls.[5] All mice were maintained on a 12:12-h light-dark cycle (lights on at 06:00). At 5–6 weeks of age, male wild-type C57BL/6J mice were fed an HFD (60% fat calories, 20% protein calories, and 20% carbohydrate calories) or a low fat diet (LFD, 10% fat calories, 20% protein calories, and 70% carbohydrate calories) for 12 weeks as previously described (7, 8). After the feeding regimen, mice were fasted for 4 h before sacrifice for collection of blood and tissue samples (38, 39). Epididymal, mesenteric, and perinephric fat depots were dissected and weighed as abdominal fat mass (39). After weighing, adipose tissue and liver samples were either fixed and embedded for histological and immunohistochemical analyses or frozen in liquid nitrogen and stored at −80 °C for further analyses. Some mice were fasted similarly and used for insulin and glucose tolerance tests and/or and insulin signaling analyses as described below. To examine the dietary effect on *in vivo* circadian clock rhythmic in relation to obesity-associated metabolic phenotypes, $mPer2^{Luc}$ mice were subjected to HFD feeding. Briefly, female homozygous $mPer2^{Luc}$ mice at 5–6 weeks of age were fed an HFD for 12

[5] S.-M. Kim, N. Neuendorff, and, D. J. Earnest, unpublished observations.

weeks. Age- and gender-matched *mPer2*^{Luc} mice were fed an LFD and used as controls. After the feeding regimen *mPer2*^{Luc} mice were subjected to the same assays used for C57BL/6J mice. Additionally, both HFD-fed and LFD-fed *mPer2*^{Luc} mice were subjected to examination of wheel-running locomotor activity rhythms as previously described (40). Some age-matched female *mPer2*^{Luc} mice were fed *ad libitum* and used for isolation of bone marrow cells.

To address a role for circadian clock rhythmic dysregulation in altering macrophage activation in relation to metabolic homeostasis, *Per1*^{ldc}/*Per2*^{ldc} mice were used for the present study. Accordingly, *Per1*^{ldc}/*Per2*^{ldc} mice (129J background) and wild-type 129J mice were maintained on a 12:12-h light-dark cycle (lights on at 06:00) and fed *ad libitum*. At 5–6 weeks of age, male *Per1*^{ldc}/*Per2*^{ldc} mice and wild-type 129J mice were anesthetized by ketamine (100 mg/kg)/xylazine (10 mg/kg of body weight). Immediately after euthanasia, *Per1*^{ldc}/*Per2*^{ldc} mice and wild-type 129J mice were subjected to isolation of bone marrow cells as previously described (24, 27). The isolated bone marrow cells were used for *in vitro* analyses and served as donor cells for bone marrow transplantation (BMT). Briefly, male wild-type C57BL/6J recipient mice at 5–6 weeks of age were lethally irradiated and subjected to BMT to generate chimeric mice using the established method (24, 26). Wild-type C57BL/6J mice that were transplanted with donor cells from *Per1*^{ldc}/*Per2*^{ldc} mice were referred to as BMT-*Per1*^{ldc}/*Per2*^{ldc} mice. Wild-type C57BL/6J mice that were transplanted with donor cells from wild-type 129J mice were referred to as BMT-WT mice. After recovery for 4 weeks, all chimeric mice were subjected for HFD feeding for 12 weeks followed by metabolic assays. All study protocols were reviewed and approved by the Institutional Animal Care and Use Committee of Texas A&M University.

Macrophage Differentiation and Characterization—Bone marrow cells were isolated from the tibias and femurs of LFD- and/or HFD-fed *mPer2*^{Luc} mice as previously described (23). After differentiation with Iscove's modified Dulbecco's medium containing 10% fetal bovine serum and 15% L929 culture supernatant for 8 days, bone marrow-derived macrophages (BMDMs) were subjected to inflammatory assays and circadian rhythm analyses using a lumicycle. Similarly, bone marrow cells were isolated from chow diet-fed *Per1*^{ldc}/*Per2*^{ldc} mice and 129J WT control mice and differentiated into BMDM for FACS analyses using flow cytometry with fluorescence-conjugated antibodies against F4/80 and CD11b as well as CD11c and CD206. For PPARγ rescue experiment, *Per1*^{ldc}/*Per2*^{ldc} BMDM were treated with a PPARγ2-expressing lentiviral vector or a control vector for 24 h according to procedures provided with commercial kits (GenTarget Inc, San Diego, CA). WT BMDM (129J background) were treated similarly with a control vector and served as the control (Ctrl). Untreated WT BMDM were also included as controls. After incubation for an additional 24 h, the treated BMDM were subjected to inflammatory analyses. To examine macrophage proinflammatory activation, BMDM were treated with LPS (100 ng/ml) or PBS for 30 min before cell harvest to examine the inflammatory signaling using Western blot analyses. Some cells were treated with or without LPS at the same dose for 6 h before harvest of RNA samples. Some cells were subjected to FACS analyses as described below.

Confirmation of Per1/2 Disruption—Genomic DNA was prepared from the tails of *Per1*^{ldc}/*Per2*^{ldc} mice and 129J wild-type mice as well as bone marrow cells, bone marrow-derived macrophages, and adipose tissue and liver samples of chimeric mice and subjected to PCR genotyping using previously described methods (41).

Insulin and Glucose Tolerance Tests—Mice were fasted for 4 h and intraperitoneally injected with insulin (1 unit/kg of body weight) or D-glucose (2 g/kg of body weight). For insulin tolerance tests, blood samples (5 μl) were collected from the tail vein before and at 15, 30, 45, and 60 min after the bolus insulin injection. Similarly, for glucose tolerance tests blood samples were collected from the tail vein before and at 30, 60, 90, and 120 min after the glucose bolus injection (7, 8).

Measurement of Metabolic Parameters—The levels of plasma glucose, triglycerides, and free fatty acids were measured using metabolic assay kits (Sigma and BioVision, Mountain View, CA). The levels of plasma insulin were measured using ELISA kits (Crystal Chem Inc., Downers Grove, IL).

Isolation of Stromal Vascular Cells from Adipose Tissue—Adipose tissue stromal vascular cells (SVCs) were isolated using the collagenase digestion method as previously described (7, 20). After digestion and centrifugation, the pelleted cells were collected as SVC. Adipose tissue SVC from *mPer2*^{Luc} mice were subjected to bioluminescence analysis as previously described (41). SVC from HFD-fed BMT-*Per1*^{ldc}/*Per2*^{ldc} and BMT-WT mice were subjected to FACS analyses and other assays.

Circadian Properties of mPer2^{Luc} *SVC and BMDM Cells*—SVC and BMDM prepared from LFD- and/or HFD-fed *mPer2*^{Luc} mice were suspended in supplemented Dulbecco's modified Eagle's medium (DMEM) (for SVC) or Iscove's modified Dulbecco's medium (for BMDM) and then plated on 35-mm culture dishes (Corning). For both cell types, the medium was changed ~24 h after plating so as to reduce the FBS concentration to 5%, and about 12 h later cultures were exposed to medium containing 50% adult horse serum for 2 h. Thereafter, serum-shocked SVC and BMDM were maintained in serum-free recording medium containing 0.1 mM beetle luciferin (Promega), 25 units/ml penicillin, and 25 μg/ml streptomycin for bioluminescence analysis as described previously (40). Individual cultures were sealed airtight with sterile glass coverslips (VWR) and sterile silicon grease (Dow Corning). The temporal patterns of mPER2::LUC bioluminescence were analyzed using an automated 32-channel luminometer (LumiCycle; Actimetrics, Wilmette, IL) that was maintained within a standard cell culture incubator at 35 °C. Bioluminescence from individual cultures was continuously recorded with a photomultiplier tube (PMT) for ~70 s at intervals of 10 min. Because of the transient induction of bioluminescence after the medium change at the initiation of this analysis, the first cycle was excluded from data analysis. Bioluminescence data were analyzed using the Lumicycle Analysis program (Actimetrics). For each raw data set, base-line drift was removed by fitting a polynomial curve with an order equal to one less than the number of recorded cycles. Rhythm parameters were determined from

base-line-subtracted data using Levenberg-Marquardt algorithm (damped Sine) fit.

Flow Cytometry Analysis—Tibias/femurs were obtained from LFD- or HFD-fed *mPer2*^{Luc} ($n = 3$) and from chow diet-fed *Per1*^{ldc}/*Per2*^{ldc} mice and 129J wild-type mice ($n = 3$) and pooled to obtain sufficient BMDM. Epididymal fat pads were obtained from HFD-fed BMT-*Per1*^{ldc}/*Per2*^{ldc} mice and BMT-WT mice to prepare SVC samples ($n = 4–6$). BMDM and adipose tissue SVC were stained with fluorescence-tagged antibodies (anti-F4/80 and anti-CD11b for macrophages and anti-CD11c and anti-CD206 for macrophage activation as previously described (42)) and subjected to FACS analyses using BD FACSAria II flow cytometer (BD Biosciences) that is operated by Texas A&M Health Science Center College of Medicine Cell Analysis Facility. Briefly, the harvested cells were analyzed based on FSC-A and SSC-A. Live cells were then examined for F4/80 (FITC) and CD11b allophycocyanin (APC) expression. Mature macrophages (F4/80$^+$ CD11b$^+$ cells) were then gated for CD11c (phycoerythrin (PE)/Cy7) and CD206 (PE) expression (macrophage polarization). Mature macrophages that were positive for CD11c but negative for CD206 were considered as M1 macrophages (F4/80$^+$ CD11b$^+$ CD11c$^+$ CD206$^-$ cells).

Co-culture of Macrophages and Adipocytes—BMDM were prepared from *Per1*^{ldc}/*Per2*^{ldc} and 129J wild-type control mice. Adipocytes were differentiated from 3T3-L1 cells in DMEM supplemented with 10 μg/ml insulin, 1 μM dexamethasone, and 0.5 mM 3-isobutyl-1-methyl-xanthine for 48 h followed by incubation for an additional 6–8 days in growth medium supplemented with 10 μg/ml insulin (7, 43). After differentiation, adipocytes were co-cultured with BMDM at a ratio of 10:1 based on the published method (24). To examine changes in inflammatory signaling, the cells were treated with or without LPS (10 ng/ml) for 30 min before cell harvest. Some cells were treated with or without insulin (100 nM) for 30 min before harvest for determination of changes in insulin signaling. Cell lysates were prepared and used to examine inflammatory and insulin signaling using Western blot analyses. Additionally, some co-culture cells were treated with or without LPS (10 ng/ml) for 6 h and subjected to preparation of RNA samples to quantify gene expression using real-time reverse transcription PCR.

Western Blots—Lysates were prepared from frozen tissue samples and cultured cells using the lysis buffer containing 50 mm HEPES (pH 7.4), 1% Triton X-100, 50 mm sodium pyrophosphate, 0.1 m sodium fluoride, 10 mm EDTA, 10 mm sodium orthovanadate, 10 μg/ml aprotinin, 10 μg/ml leupeptin, 2 mm benzamidine, and 2 mm phenylmethylsulfonyl fluoride. The levels of JNK1/2, phospho-JNK1/2, nuclear factor κB (NF-κB) p65, phospho-p65 (Ser-536), Akt1/2, phospho-Akt (Ser-473), and PPARγ in cell lysates (15 or 50 μg/lane) were analyzed using 8% Tris-glycine gels and rabbit anti-serum as a primary antibody at a 1:1000 dilution. The blot was followed by a 1:10,000 dilution of goat anti-rabbit horseradish peroxidase-conjugated secondary antibody kit (Immobilon^{TM} Western; EMD Millipore, Billerica, MA) as previously described (39). GAPDH or β-actin was used as a loading control. The maximum intensity of each band was quantified using ImageJ software. Ratios of PJNK1/JNK1 and phospho-p65/p65 as well as phospho-Akt/Akt were normalized to GAPDH or β-actin and adjusted relative to the average of control (PBS)-treated LFD, wild type, *Per1*^{ldc}/*Per2*^{ldc}, BMT-WT, or Adi/wild type, which was arbitrarily set as 1 (arbitrary units).

RNA Isolation, Reverse Transcription, and Real-time PCR—The total RNA was isolated from frozen tissue samples and cultured/isolated cells. Reverse transcription was performed using the GoScript^{TM} Reverse Transcription System (Promega), and real-time PCR analysis was performed using SYBR Green (ABI Prism 7200 Sequence Detection System; Applied Biosystems) (44, 45). The mRNA levels were analyzed for interleukin-1β (IL-1β), IL-6, tumor necrosis factor α (TNFα), IL-10, arginase1, monocyte chemoattractant protein 1 (MCP1), TLR4, adiponectin, hormone-sensitive lipase, resistin, sterol regulatory element-binding protein 1c (SREBP1c), acetyl-CoA carboxylase 1, fatty acid synthase (FAS), glucokinase, and glucose-6-phosphatase in tissue and/or cell samples. A total of 0.1 μg of RNA was used for the determination. Results were normalized to 18 S ribosomal RNA or β-actin mRNA and plotted as relative expression to the average of control (PBS)-treated LFD, wild type, *Per1*^{ldc}/*Per2*^{ldc}, BMT-WT, or Adi/wild-type, which was arbitrarily set as 1.

Statistical Methods—Numeric data are presented as the means ± S.E. Statistical significance was assessed by unpaired, two-tailed analysis of variance or Student's *t* tests. Differences were considered significant at the two-tailed $p < 0.05$.

RESULTS

HFD Feeding Induces Adiposity, Adipose Tissue Inflammation, Systemic Insulin Resistance, and Circadian Clock Dysregulation—Consistent with established observations (4, 5, 7), HFD-fed C57BL/6J mice displayed increased adiposity, adipose tissue inflammation, and systemic insulin resistance (data not shown). To address a possible link between metabolic phenotype and alterations in circadian clock function, homozygous *mPer2*^{Luc} knockin mice (C57BL/6J background) were subjected to an identical feeding regimen. After HFD feeding for 12 weeks, *mPer2*^{Luc} mice exhibited a marked increase in body weight and abdominal fat mass compared with LFD-fed mice (Fig. 1, *A* and *B*). Additionally, HFD-fed *mPer2*^{Luc} mice exhibited a significant increase in the severity of insulin resistance and glucose intolerance (Fig. 1, *C* and *D*) as well as an increase in the period of the circadian rhythm of wheel-running behavior (Fig. 1*E*).

HFD Feeding Lengthens the Period of Clock Gene Oscillations in Adipose Tissue Stromal Vascular Cells and Bone Marrow-derived Macrophages and Increases Macrophage Proinflammatory Activation—Given the role of macrophages in inflammation (5, 7), we analyzed circadian oscillations of the clock gene *Per2* in adipose tissue SVC, the immune cell-containing fraction of collagenase-digested visceral fat that has been widely used to examine the inflammatory status of adipose tissue macrophages (5, 23), and BMDM derived from *mPer2*^{Luc} mice. SVC cultures from LFD-fed mice exhibited robust mPER2::LUC rhythms with a circadian period of 25.06 ± 0.4 h (Fig. 2*A*). However, SVC cultures from HFD-fed mice were characterized by mPER2::LUC rhythms in which the period was significantly increased by ~9 h (Fig. 2*A*). Similarly, the period of BMDM

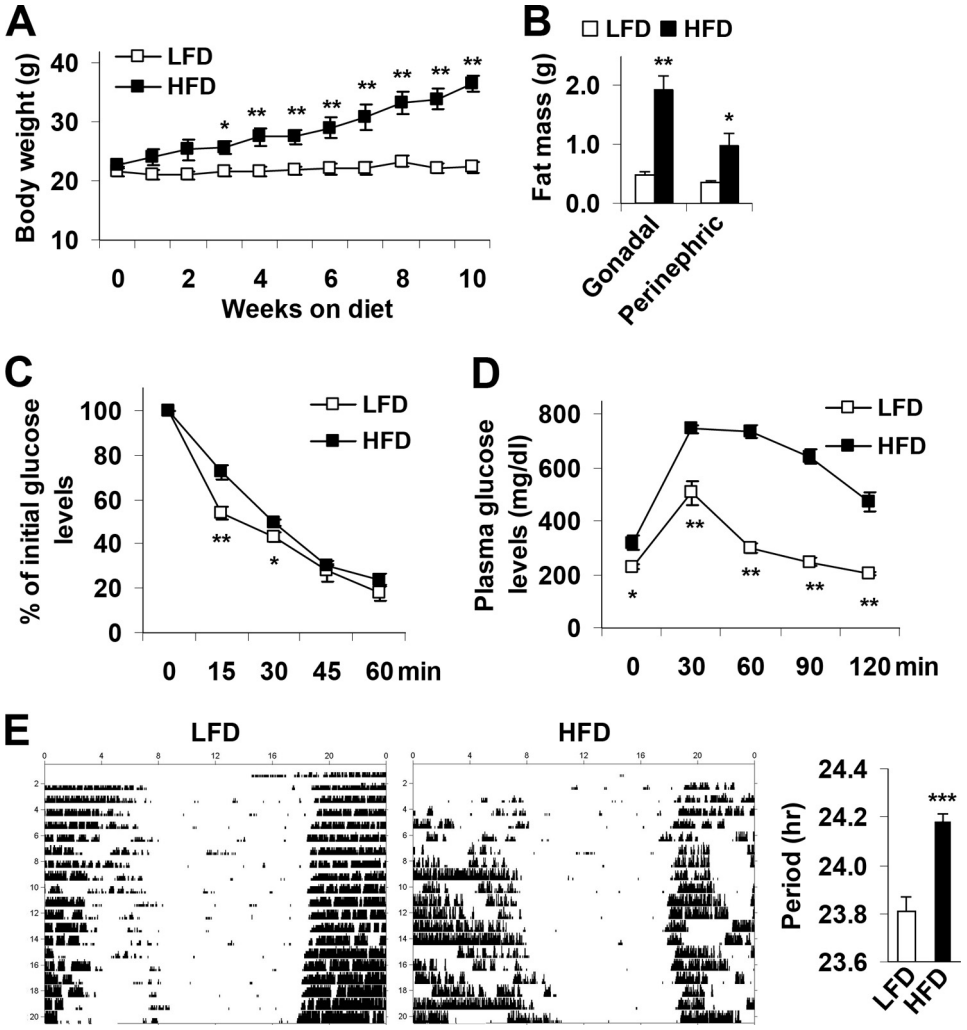

FIGURE 1. **Over-nutrition induces obesity-associated circadian clock dysregulation.** At 5–6 weeks of age, *mPer2*^{Luc} mice were fed an HFD or a LFD for 12 weeks ($n = 5$–10). *A*, body weight was recorded weekly during the feeding regimen. *B*, adipose mass. Abdominal fat mass was calculated from the sum of gonadal and perinephric fat content. *C*, insulin tolerance tests. *D*, glucose tolerance tests. *E*, representative circadian rhythms of wheel-running activity in LFD- and/or HFD-fed mice during exposure to constant darkness. The *bar graph* depicts differences in the free-running period of the activity rhythm between treatment groups. For *A–E*, data are the means ± S.E. in line and bar graphs. *, $p < 0.05$; **, $p < 0.01$; ***, $p < 0.001$, HFD *versus* LFD (*E*, *right panel*) for the same time point (*A*, *C*, and *D*) or the same fat pad (*B*). For *B–D*, mice were fasted for 4 h starting at the same time of the day before tissue collection or physiological assays. For *C* and *D*, mice were given a peritoneal injection of insulin (1 unit/kg) (*C*) or glucose (2 g/kg) (*D*).

rhythms in mPER2::LUC bioluminescence was significantly increased in cultures from HFD-fed *mPer2*^{Luc} mice relative to those from LFD-fed mice (Fig. 2*B*). BMDM cultures from HFD-fed *mPer2*^{Luc} mice were also distinguished by robust decreases in the amplitude of the mPER2::LUC rhythm. When the inflammatory status was analyzed under basal conditions (PBS-treated), the phosphorylation of JNK1 (p46, the key JNK isoform that mediates proinflammatory signaling) and NF-κB p65 in BMDM from HFD-fed *mPer2*^{Luc} mice did not significantly differ from that in BMDM from LFD-fed mice. However, upon LPS treatment, the phosphorylation of JNK1 and NF-κB p65 (Ser-536) in BMDM from HFD-fed *mPer2*^{Luc} mice was significantly increased by 2.1- and 1.6-fold, respectively, compared with that in BMDM from LFD-fed mice (Fig. 2*C*). Moreover, under both basal and LPS-treated conditions, IL-1β, IL-6, and TNFα mRNA levels in BMDM from HFD-fed *mPer2*^{Luc} mice were increased significantly relative to their respective levels in BMDM from LFD-fed mice (Fig. 2*D*). Thus, over-nutrition increases macrophage proinflammatory activation in concert with its effects on altering the timekeeping function of the macrophage circadian clockworks.

Circadian Clock Disruption Increases Macrophage Proinflammatory Activation—To address a direct role for circadian clock disruption in altering macrophage inflammatory status, BMDM obtained from mutant mice with targeted disruption of the clock genes *Per1* and *Per2* (*Per1*^{ldc}/*Per2*^{ldc}, 129J background) characterized by a loss of circadian rhythmicity (37) and from WT 129J mice were subjected to FACS analyses. Among the analyzed cells, >95% of a total of 20,000–30, 000 cells were mature macrophages (F4/80$^+$ CD11b$^+$ cells) (Fig. 3*A*, quantitative data not included). Mature macrophages were then examined for activation status based on CD11c and CD206 expression (Fig. 3*B*). Compared with controls, BMDM from *Per1*^{ldc}/*Per2*^{ldc} mutant mice displayed a significantly higher percentage of proinflammatory (M1) macrophages (F4/80$^+$ CD11b$^+$ CD11c$^+$ CD206$^-$ cells) and no difference in percentage of anti-inflammatory (M2) macrophages (F4/80$^+$ CD11b$^+$ CD11c$^-$ CD206$^+$ cells) (Fig. 3*C*). When inflammatory

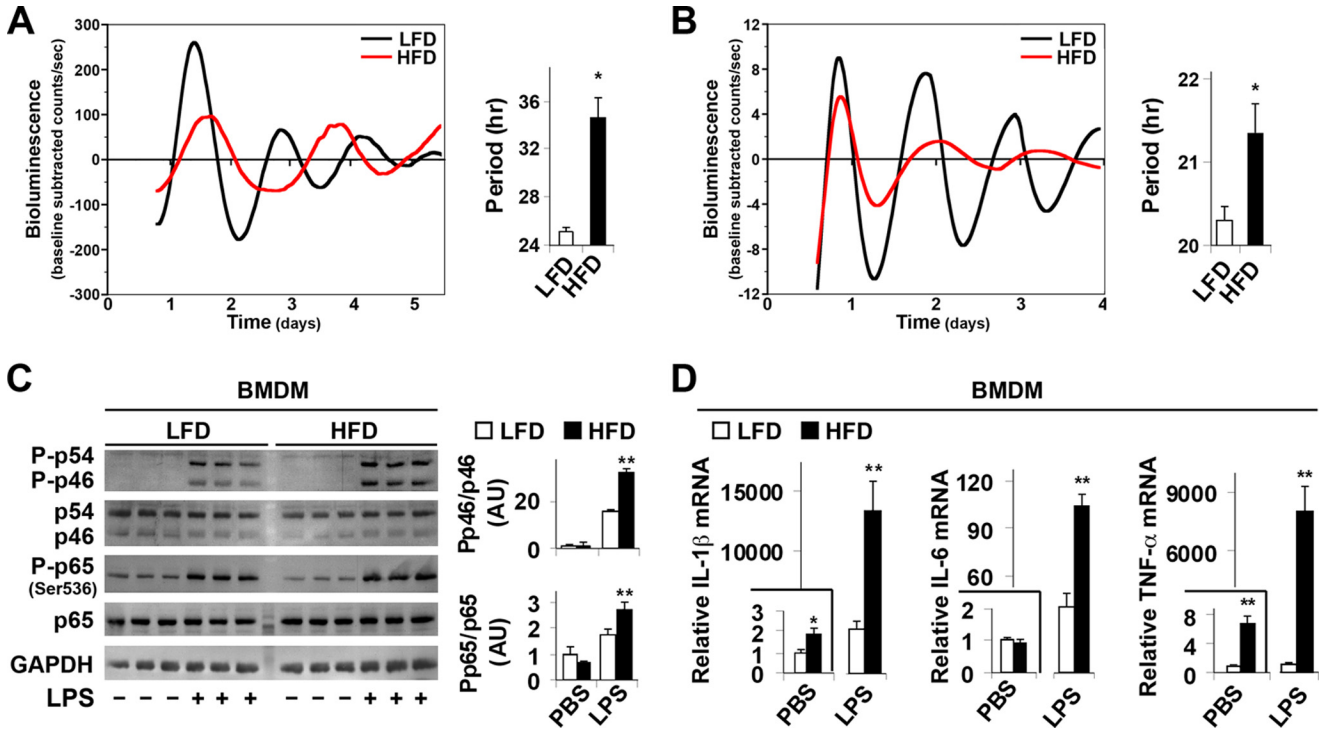

FIGURE 2. **Over-nutrition lengthens the period of clock gene oscillations in adipose tissue SVC and in macrophages and enhances macrophage proinflammatory activation.** At 5–6 weeks of age, *mPer2*^{Luc} mice were fed an HFD or LFD for 12 weeks (n = 5–6). *A* and *B*, representative recordings of ensemble PER2::LUC bioluminescence (expressed as detrended base-line-subtracted counts per second) from cultured adipose tissue SVC (*A*) or BMDM (*B*). *Bar graphs* depict group differences in PER2::LUC rhythm period between treatment groups. *C*, macrophage inflammatory signaling. Before harvest, BMDM were treated with LPS (100 ng/ml) or PBS for 30 min. The levels of JNK1 (p46), phospho-JNK1, NF-κB p65, and phospho-p65 (Ser-536) were examined using Western blot analyses and quantified using densitometry. *D*, macrophage IL-1β, IL-6, and TNF-α mRNA expression. Before harvest, BMDM were treated with LPS (100 ng/ml) or PBS for 6 h. IL-1β and TNF-α mRNA levels were quantified using real-time PCR and plotted as relative expression. For *bar graphs* (*A–D*), data are the means ± S.E. *, $p < 0.05$; **, $p < 0.01$ HFD *versus* LFD (*A* and *B*) under the same conditions (PBS or LPS) (*C* and *D*).

signaling was examined under basal conditions (PBS-treated), BMDM levels of JNK1 phosphorylation remained low with no genotype-based differences (Fig. 3*D*). However, in response to LPS, the phosphorylation of JNK1 in BMDM from *Per1*^{ldc}/*Per2*^{ldc} mice was significantly increased compared with that in BMDM from WT mice. Additionally, under both basal and LPS-treated conditions, NF-κB p65 phosphorylation (Ser-536) in BMDM from *Per1*^{ldc}/*Per2*^{ldc} mice was significantly higher than that in BMDM from WT mice. Among proinflammatory cytokines that were examined, IL-1β and TNFα mRNA expression in BMDM under both basal and LPS-treated conditions differed in accord with genotype (Fig. 3*E*). Compared with controls, BMDM from *Per1*^{ldc}/*Per2*^{ldc} mice exhibited significant increases in both basal and LPS-induced expression of IL-1β and TNFα mRNA. The levels of IL-6 mRNA did not differ between genotypes. Thus, circadian clock malfunction associated with targeted disruption of *Per 1* and *Per 2* recapitulates macrophage proinflammatory activation induced by over-nutrition (Fig. 2).

PPARγ2 Overexpression Ameliorates Per1/2 Disruption-associated Macrophage Proinflammatory Activation—In subsequent mechanistic analyses, we next examined the expression of PPARγ because activation of this transcription factor stimulates macrophage alternative (anti-inflammatory) activation (20, 23), and its promoter region contains multiple E-boxes that bind the basic helix-loop-helix protein complexes formed by the core elements of the molecular clock brain muscle ARNT-like protein 1 (BMAL1) and circadian locomotor output cycles kaput (CLOCK) (46). PPARγ protein levels in BMDM from *Per1*^{ldc}/*Per2*^{ldc} mice were significantly decreased by 40–60% relative to that observed in untreated and control vector-treated WT BMDM (Fig. 4*A*). To address the potential involvement of PPARγ in *Per1/2* regulation of macrophage activation, we next determined whether overexpression of PPARγ2, one of the two PPARγ isoforms that effectively mediates PPARγ actions (47), ameliorates the inflammatory status of BMDM from *Per1*^{ldc}/*Per2*^{ldc} mice. In comparison with cultures infected with a control vector, PPARγ2 overexpression in *Per1*^{ldc}/*Per2*^{ldc}-derived BMDM significantly increased PPARγ content by 2.5-fold (Fig. 4*A*) and significantly reduced the phosphorylation of JNK1 and NF-κB p65 (Ser-536) in response to LPS treatment (Fig. 4*B*). IL-1β and TNFα mRNA levels were similar under basal conditions in *Per1*^{ldc}/*Per2*^{ldc} controls and PPARγ2-overexpressing *Per1*^{ldc}/*Per2*^{ldc} BMDM. However, the LPS-mediated induction of IL-1β and TNFα, but not IL-6, mRNA levels in PPARγ2-overexpressing *Per1*^{ldc}/*Per2*^{ldc} BMDM was significantly decreased relative to that found in control-treated *Per1*^{ldc}/*Per2*^{ldc} BMDM (Fig. 4*C*). Consistent with these observations, FACS analysis revealed that among analyzed mature macrophages, *Per1*^{ldc}/*Per2*^{ldc} controls showed a higher percentage of M1 macrophages compared with WT control cells. Importantly, PPARγ2 overexpression in *Per1*^{ldc}/*Per2*^{ldc} BMDM induced a significant decrease in the percentage of M1 macrophages relative to that observed in control-treated cells

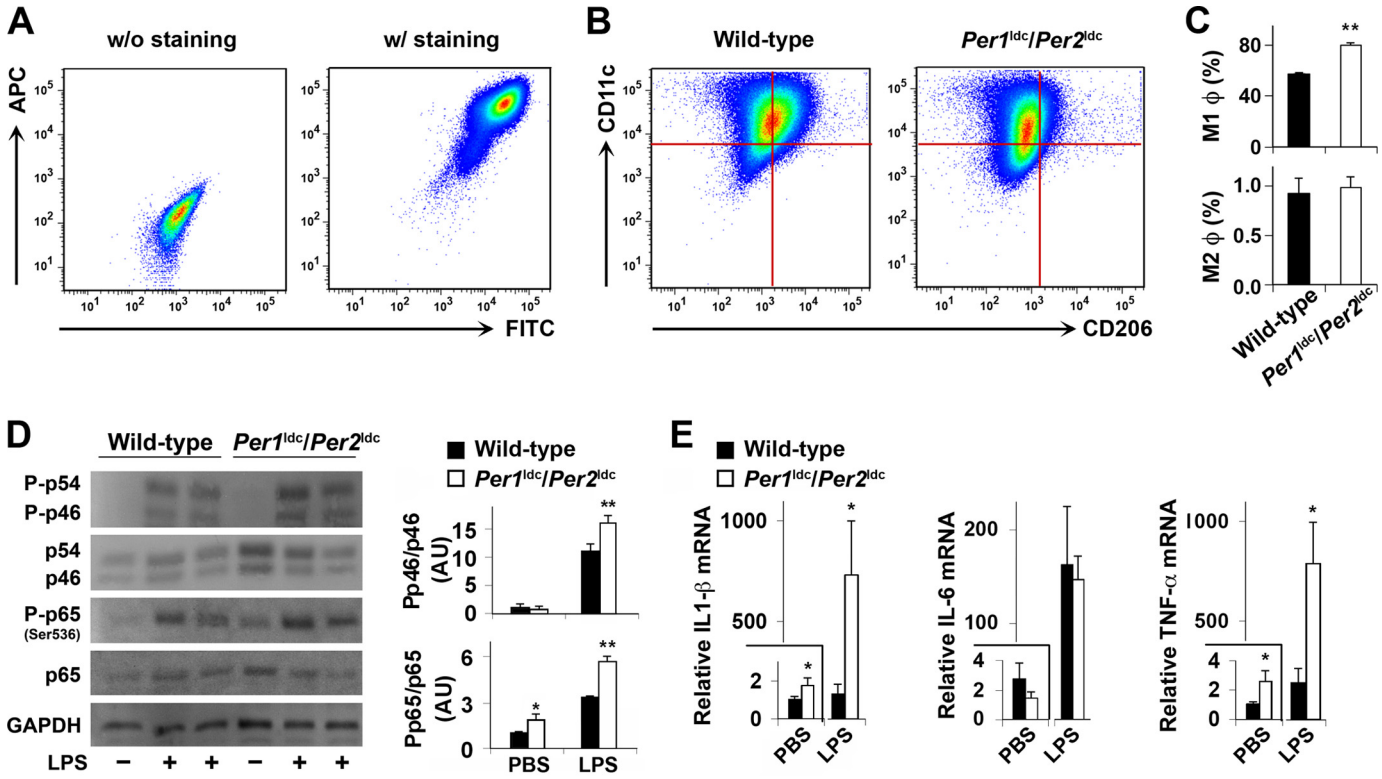

FIGURE 3. ***Per1/2* disruption increases macrophage proinflammatory activation.** BMDM were prepared from chow diet-fed wild-type mice and *Per1*^{ldc}/*Per2*^{ldc} mice with targeted disruption of the clock genes *Per1* and *Per2* ($n = 4–6$). *A*, representative plots of macrophage purity and gating. BMDM were included without (*left panel*) or with (*right panel*) FITC-labeled anti-F4/80 and allophycocyanin (*APC*)-labeled anti-CD11b antibodies and examined for FITC and APC intensities. *B* and *C*, BMDM were examined for F4/80 and CD11b expression. Mature macrophages (F4/80$^+$ CD11b$^+$ cells) were then gated for CD11c and CD206 expression. *Panels* in *B*, representative plots of proinflammatory (*M1*) macrophages (F4/80$^+$ CD11b$^+$ CD11c$^+$ CD206$^-$ cells) and anti-inflammatory (*M2*) macrophages (F4/80$^+$ CD11b$^+$ CD11c$^-$ CD206$^+$ cells); *bar graph* in *C*, *top panel* for the percentages of M1 macrophages (*upper left quadrant of panels in B*) in mature macrophages and *bottom panel* for M2 macrophages (*bottom right quadrant of panels in B*). *D*, macrophage inflammatory signaling. Before harvest BMDM were treated with LPS (100 ng/ml) or PBS for 30 min. The levels of total and phosphorylated JNK1 (p46) and NF-κB p65 were examined using Western blot analyses and quantified using densitometry. *E*, macrophage mRNA levels of proinflammatory cytokines. Before harvest, BMDM were treated with LPS (100 ng/ml) or PBS for 6 h. The mRNA levels of IL-1β, IL-6, and TNFα were quantified using real-time PCR and plotted as relative expression. For *bar graphs* (*C–E*), data are the means ± S.E. *, $p < 0.05$; **, $p < 0.01$ *Per1*^{ldc}/*Per2*^{ldc} *versus* wild-type (*C*) under the same conditions (PBS or LPS) (*D* and *E*).

(Fig. 4*D*). Among three groups of BMDM (control-treated WT, control-treated *Per1*^{ldc}/*Per2*^{ldc}, PPARγ2-overexpressing *Per1*^{ldc}/*Per2*^{ldc}), the percentages of M2 macrophages did not differ significantly. Thus, PPARγ may play a role in the mechanism by which *Per1/2* disruption up-regulates macrophage proinflammatory activation.

Myeloid Cell-specific Per1/2 Disruption Exacerbates Adipose Tissue Inflammation in Obesity—The inflammatory status of macrophages governs the outcome of adipose tissue inflammation and thereby systemic insulin sensitivity (22, 23). To address the impact of macrophage-specific circadian clock on HFD-induced adipose tissue inflammation, bone marrow cells were isolated from *Per1*^{ldc}/*Per2*^{ldc} mutant and WT mice and then transplanted into lethally irradiated WT recipient (C57BL/6J) mice (BMT). After HFD feeding for 12 weeks and subsequent and metabolic characterization, bone marrow cells, BMDM, and adipose-derived SVC as well as adipose and liver tissues from chimeric mice were genotyped to identify WT and targeted alleles (*Per1*, *Per2*) and confirm bone cell repopulation. In BMT-WT mice (recipients, WT C57BL/6J mice; donors, WT 129J mice), genotyping of all genomic DNA samples revealed PCR products for only WT alleles (Fig. 5, *A–E*). In contrast, genomic DNA from all of these tissues/cells except BMDM in BMT-*Per1*^{ldc}/*Per2*^{ldc} mice (recipients, WT C57BL/6J mice; donors, *Per1*^{ldc}/*Per2*^{ldc} mice) showed PCR products for WT and mutant alleles. Genotyping of BMDM genomic DNA from BMT-*Per1*^{ldc}/*Per2*^{ldc} mice only yielded PCR products for mutant alleles (Fig. 5*B*). These results demonstrate the success of adoptive transfer of *Per1/2*-disrupted myeloid cells to WT recipient mice.

When adipose tissue inflammatory status was examined, the phosphorylation of JNK1 and NF-κB p65 (Ser-536) in HFD-fed BMT-*Per1*^{ldc}/*Per2*^{ldc} mice was significantly increased (Fig. 6*A*) compared with that in HFD-fed BMT-WT. Additionally, adipose tissue IL-1β, IL-6, and TNFα mRNA levels in HFD-fed BMT-*Per1*^{ldc}/*Per2*^{ldc} mice were significantly higher than their respective levels in HFD-fed BMT-WT mice (Fig. 6*B*), whereas BMT genotype had no significant effect on the mRNA levels of arginase 1 and IL-10, which are indicative of macrophage alternative activation. Next, adipose-derived SVC were subjected to FACS analyses. After HFD feeding, SVC of BMT-*Per1*^{ldc}/*Per2*^{ldc} mice displayed a 1.8-fold increase in mature macrophages (F4/80$^+$ CD11b$^+$ cells) compared with those of BMT-WT mice (Fig. 6*C*). Upon analyzing the inflammatory status of the mature macrophages, adipose tissue SVC isolated from BMT-*Per1*^{ldc}/*Per2*^{ldc} mice showed a 2-fold increase in the overall percentage of proinflammatory macrophages (F4/80$^+$ CD11b$^+$ CD11c$^+$ CD206$^-$ cells) relative to that observed in

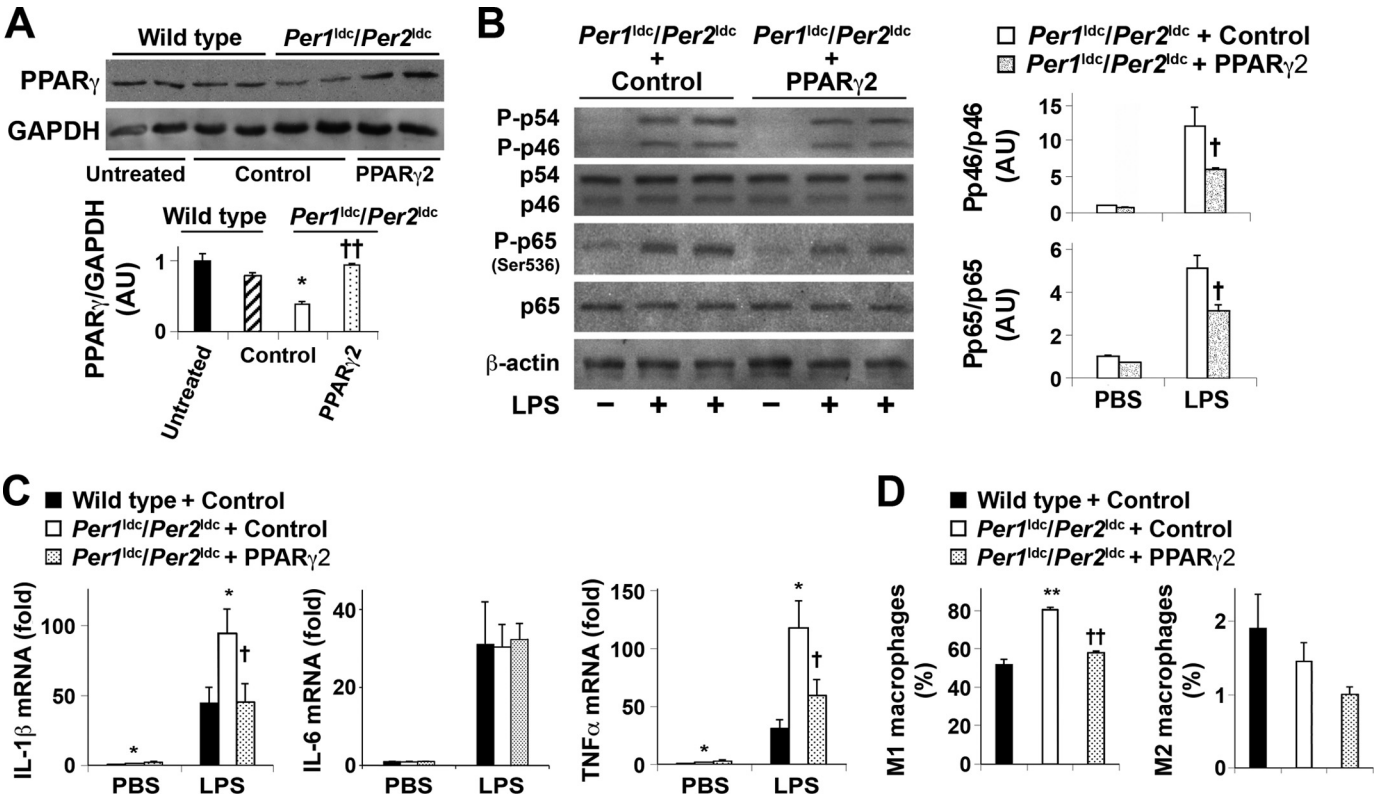

FIGURE 4. **PPARγ2 overexpression ameliorates *Per1/2* disruption-associated macrophage proinflammatory activation.** BMDM were prepared from chow diet-fed wild-type mice and *Per1*^{ldc}/*Per2*^{ldc} mice with targeted disruption of the clock genes *Per1* and *Per2* ($n = 4–8$). *A*, lysates of untreated macrophages as well as PPARγ2-expressing-lentivirus- and/or control-lentivirus-treated macrophages were examined for PPARγ content. For the *bar graph*, PPARγ content was examined using Western blot analyses and quantified using densitometry. *B*, macrophage inflammatory signaling. Before harvest, BMDM were treated with LPS (100 ng/ml) or PBS for 30 min. The levels of total and phosphorylated JNK1 (p46) and NF-κB p65 were examined using Western blot analyses and quantified using densitometry. *C*, macrophage levels of IL-1β, IL-6, and TNFα mRNA. Before harvest, BMDM were treated with LPS (100 ng/ml) or PBS for 6 h. The mRNA levels of cytokines were quantified using real-time PCR and plotted as relative expression. *D*, the percentages of M1/M2 macrophages were examined using FACS analysis. For *A–D*, *Per1*^{ldc}/*Per2*^{ldc}-BMDM were infected with a lentivirus containing the cDNA of human PPARγ2 or a control lentivirus at 6 days after differentiation for 24 h. Control vector-treated WT BMDM were included for comparison. The infected cells were incubated for an additional 48 h and subjected to the pertinent assays. For *bar graphs* (*A–D*), data are the means ± S.E. *, $p < 0.05$; **, $p < 0.01$ *Per1*^{ldc}/*Per2*^{ldc} *versus* wild-type for infected cells (*A* and *D*) under the same conditions (*C*); †, $p < 0.05$ and †† $p < 0.01$ *Per1*^{ldc}/*Per2*^{ldc} + PPARγ2 *versus* *Per1*^{ldc}/*Per2*^{ldc} (*A* and *D*) under LPS-treated condition (*B* and *C*). *AU*, arbitrary units.

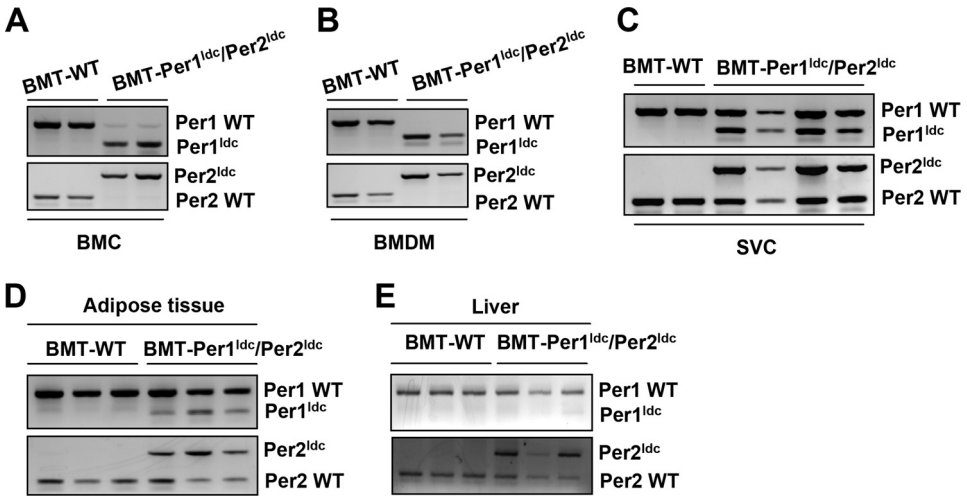

FIGURE 5. **Confirmation of bone marrow cell repopulation.** Bone marrow cells from WT 129J mice and *Per1*^{ldc}/*Per2*^{ldc} (129J background) mice were transplanted into lethally irradiated male WT C57BL/6J mice (at 5–6 weeks of age). After recovery for 4 weeks, chimeric mice (*BMT-WT* and *BMT-Per1*^{ldc}/*Per2*^{ldc}) were fed an HFD for 12 weeks. After the feeding regimen, genomic DNA was isolated from both isolated cells, and tissue samples were obtained from all chimeric mice and then subjected to PCR genotyping analyses to identify WT and targeted alleles (*Per1*, *Per2*) and confirm bone cell repopulation. The amplified band of smaller size (~235 bp, *top panel*) signifies the *Per1* targeted alleles, whereas the PCR product of larger size (~403 bp, *bottom panel*) denotes the *Per2* targeted alleles in bone marrow cells (*A*), BMDM (*B*), adipose tissue SVC (*C*), adipose tissue (*D*), and liver (*E*).

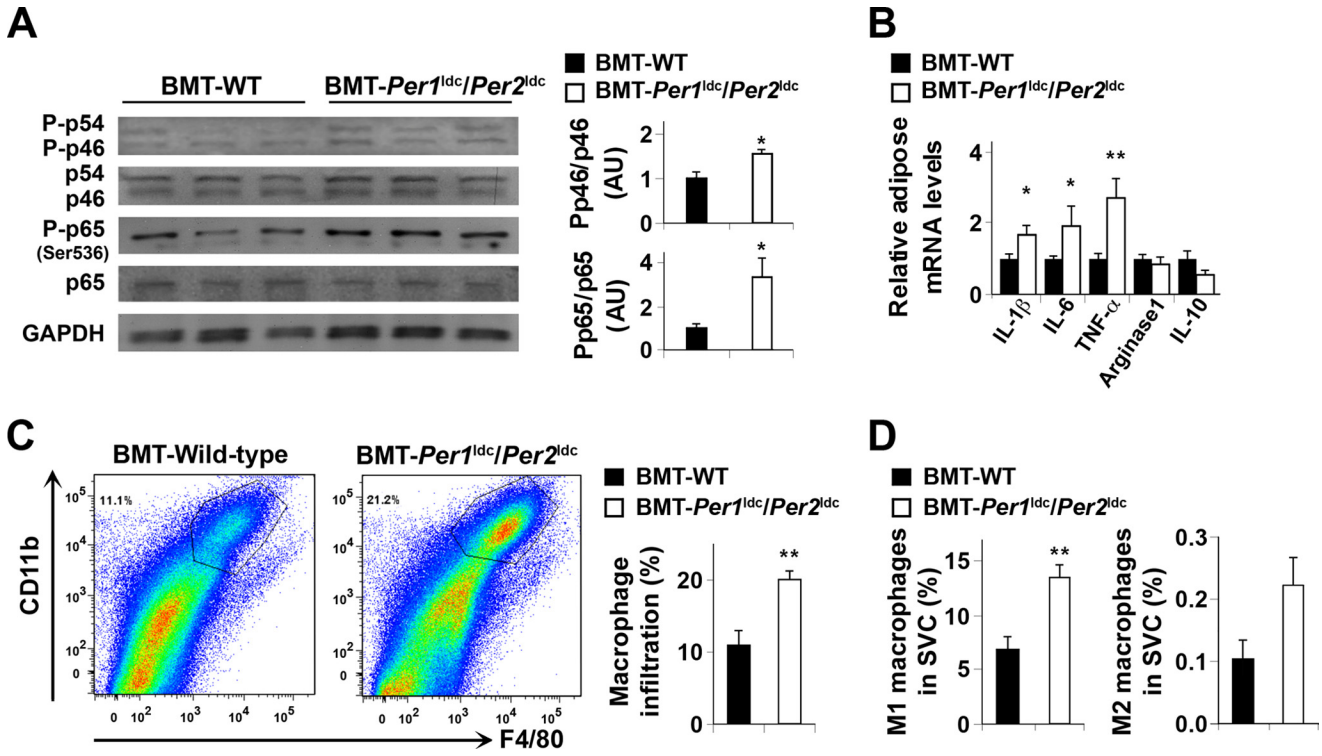

FIGURE 6. **Myeloid cell-specific *Per1/2* disruption exacerbates HFD-induced adipose tissue inflammation.** Chimeric mice (*BMT-WT* and *BMT-Per1*^{ldc}/*Per2*^{ldc}) were fed an HFD for 12 weeks ($n = 6–10$). Before tissue collection, mice were fasted for 4 h starting at the same time of the day. *A*, adipose tissue inflammatory signaling. The levels of total and phosphorylated JNK1 (p46) and NF-κB p65 were examined using Western blot analyses and quantified using densitometry. *B*, adipose tissue expression of genes related to macrophage polarization. The mRNA levels of cytokines and arginase1 were quantified using real-time PCR and plotted as relative expression. *C*, FACS analyses of macrophage infiltration in epididymal fat pads of HFD-fed chimeric mice. *Left two panels*, representative plots of adipose tissue SVC that were quantified for F4/80 and CD11b expression; *right panel*, percentages of mature macrophages (F4/80$^+$ CD11b$^+$ cells). *D*, quantification of proinflammatory (*M1*) macrophages (F4/80$^+$ CD11b$^+$ CD11c$^+$ CD206$^-$ cells), and anti-inflammatory (*M2*) macrophages (F4/80$^+$ CD11b$^+$ CD11c$^-$ CD206$^+$ cells) in SVC isolated from adipose tissue of HFD-fed chimeric mice. For *bar graphs* (*A–D*), data are the means ± S.E. *, $p < 0.05$; **, $p < 0.01$ BMT-*Per1*^{ldc}/*Per2*^{ldc} *versus* BMT-WT (*A*, *C*, and *D*) for the same gene (*B*). *AU*, arbitrary units.

BMT-WT mice (Fig. 6*D*). In contrast, the percentage of M2 macrophages in adipose tissue SVC did not differ between the WT and mutant groups. Thus, myeloid cell-specific *Per1/2* disruption increases adipose tissue infiltration of proinflammatory macrophages, thereby exacerbating HFD-induced adipose tissue inflammatory responses.

Myeloid Cell-specific Per1/2 Disruption Exacerbates Adiposity and Adipose Tissue Dysfunction—Next, we examined the effects of myeloid cell-specific circadian clock disruption on adipose tissue metabolic responses in WT recipients. In response to HFD feeding, BMT-*Per1*^{ldc}/*Per2*^{ldc} mice gained much more abdominal fat mass and displayed a greater increase in adiposity than BMT-WT mice (Fig. 7, *A* and *B*). Consistent with these changes, the size of most adipocytes in adipose tissue was larger in BMT-*Per1*^{ldc}/*Per2*^{ldc} mice than in BMT-WT mice (Fig. 7*C*). Locally, adipose tissue of HFD-fed BMT-*Per1*^{ldc}/*Per2*^{ldc} mice showed a significant decrease in insulin-induced Akt phosphorylation (Ser-473) relative to that observed in HFD-fed BMT-WT mice (Fig. 7*D*), and this decrease was accompanied by decreased adipose tissue expression of mRNAs encoding adiponectin, an adipokine that improves systemic insulin sensitivity, and hormone-sensitive lipase (Fig. 7*E*), a rate-determining enzyme that controls adipose tissue fat deposition by hydrolyzing triglycerides stored in adipose tissue lipid droplets. Compared with HFD-fed BMT-WT mice, HFD-fed BMT-*Per1*^{ldc}/*Per2*^{ldc} mice also showed a significant increase in adipose tissue mRNA levels of resistin, an adipokine that promotes systemic insulin resistance (Fig. 7*E*); although adipose tissue mRNA levels of MCP1, whose increase in adipocytes attracts macrophage infiltration, and TLR4, an inflammatory receptor, did not differ between HFD-fed BMT-*Per1*^{ldc}/*Per2*^{ldc} mice and BMT-WT mice. Together, these results indicate that myeloid cell-specific *Per1/2* disruption potentiates HFD-induced adipose tissue dysfunction.

Per1/2-disrupted Macrophages Increase Adipocyte Inflammatory Responses and Impair Adipocyte Functions—Given the critical role of macrophages in initiating or exacerbating adipose tissue inflammation, we co-cultured macrophages and adipocytes at a 1:10 ratio to address the direct effects of circadian clock disruption on macrophages and/or macrophage factors that regulate adipocyte function. Compared with co-cultures containing adipocytes and WT BMDM (Adi/WT BMDM), adipocytes cultured with *Per1*^{ldc}/*Per2*^{ldc} BMDM (Adi/*Per1*^{ldc}/*Per2*^{ldc} BMDM) showed a much greater increase in NF-κB p65 (Ser-536) phosphorylation in response to LPS treatment (Fig. 8*A*). Adipocytes cultured with *Per1*^{ldc}/*Per2*^{ldc} BMDM also exhibited a significant increase in IL-1β, IL-6, TNF-α, and resistin mRNA levels and a decrease in adiponectin mRNA levels compared with their respective levels in Adi/WT BMDM co-cultures (Fig. 8*B*), indicating increased production of pro-insulin resistant and pro-hyperglycemic factors. When insulin signaling was analyzed, adipocytes cultured with

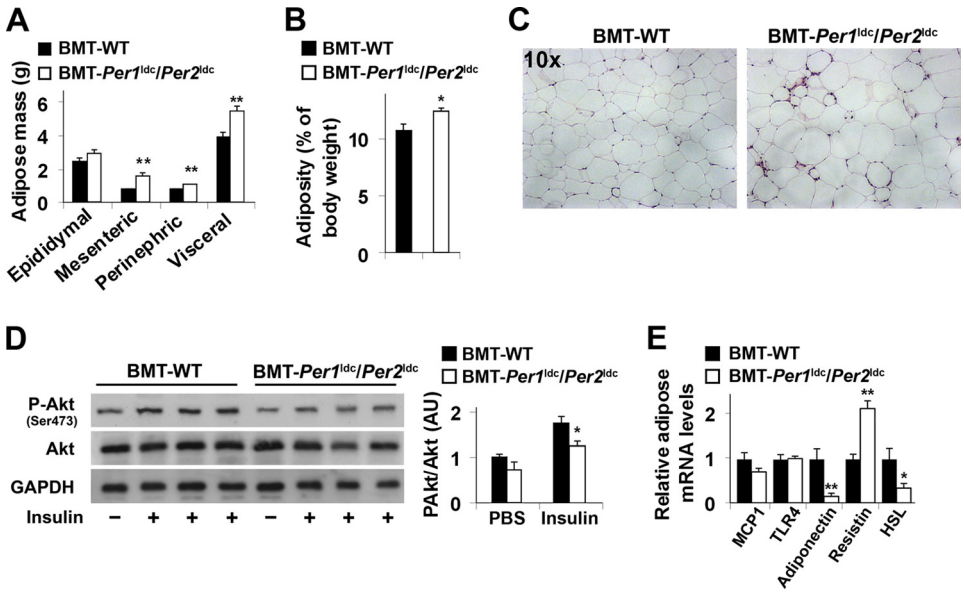

FIGURE 7. **Myeloid cell-specific *Per1/2* disruption exacerbates HFD-induced adiposity and adipose tissue insulin resistance.** Chimeric mice (BMT-WT and BMT-*Per1*^{ldc}/*Per2*^{ldc}) were fed an HFD for 12 weeks ($n = 6–10$). Before tissue collection or insulin injection, mice were fasted for 4 h starting at the same time of the day. *A*, adipose mass. Abdominal fat mass was calculated as the sum of epididymal, mesenteric, and perinephric fat content. *B*, adiposity was calculated by normalizing abdominal fat content to body weight. *C*, H&E staining of adipose tissue. *D*, adipose tissue insulin signaling. After fasting, HFD-fed chimeric mice were given a bolus injection of insulin (1 unit/kg of body weight) or PBS into the portal vein. The levels of total and phosphorylated Akt1/2 were examined using Western blot analyses and quantified using densitometry. *E*, adipose tissue gene expression. The adipose mRNA levels of genes involved in adipose tissue inflammatory and metabolic responses were quantified using real-time PCR and plotted as relative expression. For *bar graphs* (*A*, *B*, *D*, and *E*), data are the means ± S.E. *, $p < 0.05$; **, $p < 0.01$ BMT-*Per1*^{ldc}/*Per2*^{ldc} *versus* BMT-WT (*B*) for the same fat pad (*A*) or under the same condition (insulin in *D*) or for the same gene (*E*). *AU*, arbitrary units.

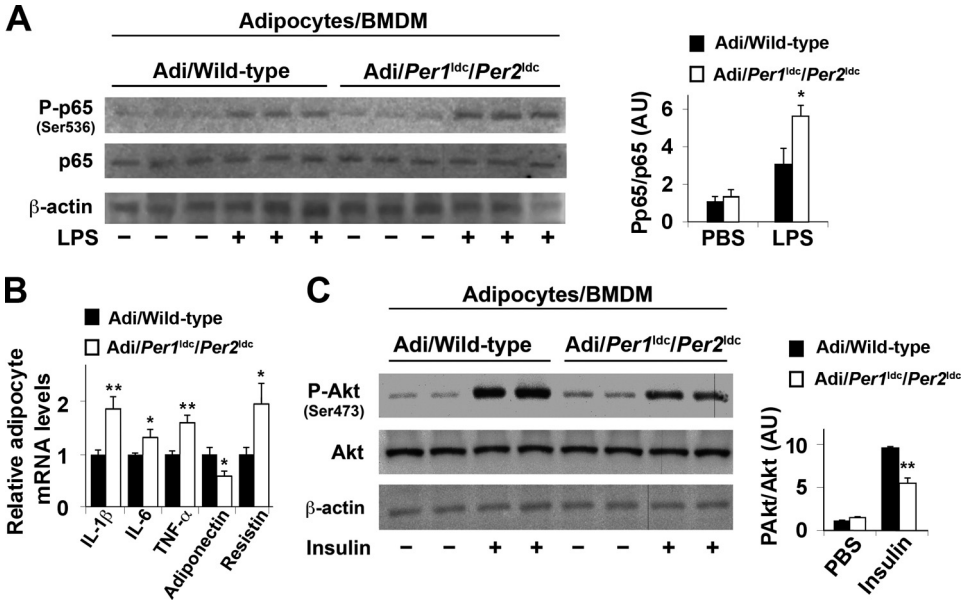

FIGURE 8. ***Per1/2*-disrupted macrophages increase adipocyte inflammatory responses and impair adipocyte insulin signaling in co-cultures.** Adipocytes were co-cultured with macrophages differentiated from bone marrow cells of wild-type (*Adi/Wild-type*) or *Per1*^{ldc}/*Per2*^{ldc} mice (*Adi/Per1*^{ldc}/*Per2*^{ldc}) at a 10:1 ratio (adipocytes:macrophages) for 48 h ($n = 4–6$). *A*, NF-κB signaling of co-cultured adipocytes. Before harvest, adipocyte-macrophage co-cultures were treated with LPS (100 ng/ml) or PBS for 30 min. The levels of total and phosphorylated NF-κB p65 were examined using Western blot analyses and quantified using densitometry. *B*, cytokine and adipokine mRNA levels in co-cultured adipocytes were quantified using real-time PCR and plotted as relative expression. *C*, insulin signaling of co-cultured adipocytes. Before harvest, the co-cultures were treated with insulin (100 nM) or PBS for 30 min. The levels of total and phosphorylated Akt1/2 were examined using Western blot analyses and quantified using densitometry. For *bar graphs*, data are the means ± S.E. *, $p < 0.05$; **, $p < 0.01$ Adi/*Per1*^{ldc}/*Per2*^{ldc} *versus* Adi/Wild-type under the same conditions (LPS in *A*; insulin in *C*) for the same gene (*B*). *AU*, arbitrary units.

Per1^{ldc}/*Per2*^{ldc} BMDM showed a significant decrease in insulin-induced Akt phosphorylation (Ser-473) compared with Adi/WT BMDM co-cultures (Fig. 8*C*). Taken together, these results suggest that *Per1/2*-disrupted macrophages directly increase adipocyte proinflammatory responses and decrease adipocyte insulin sensitivity.

Myeloid Cell-specific Per1/2 Disruption Exacerbates Diet-induced Insulin Resistance and Glucose Intolerance—Macrophage-driven adipose tissue inflammation contributes to the development of systemic insulin resistance (27, 28). We examined systemic pathophysiology. Before HFD feeding, the body weight of BMT-*Per1*^{ldc}/*Per2*^{ldc} mice did not differ from

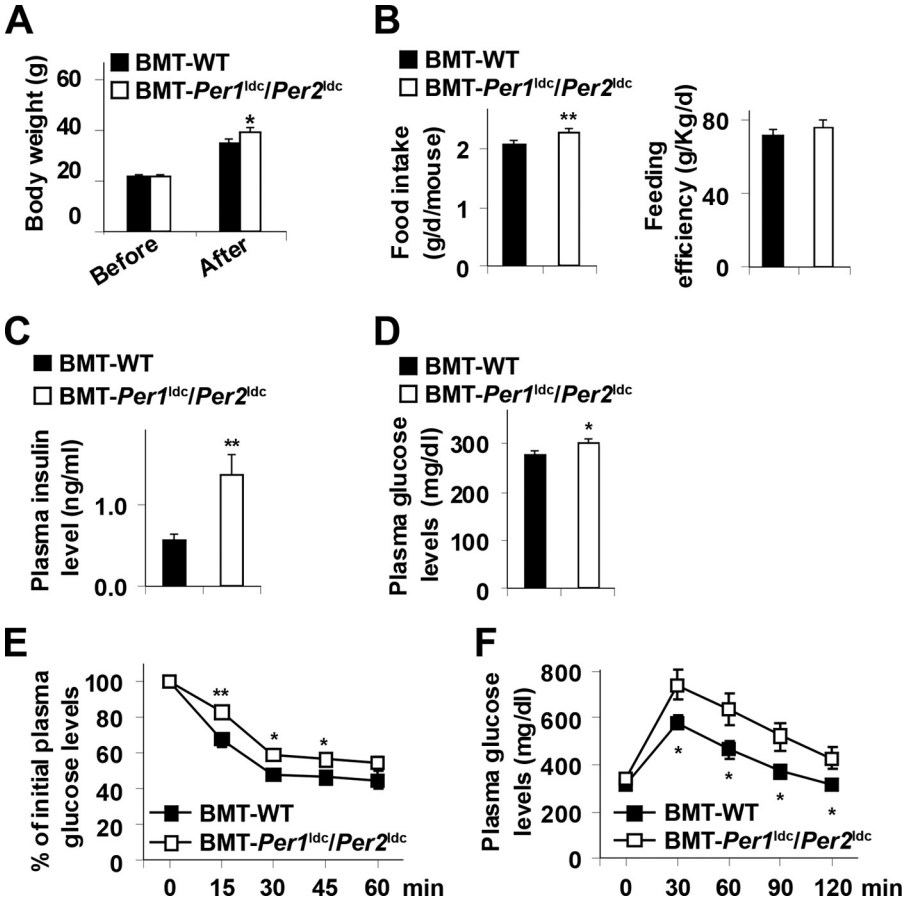

FIGURE 9. **Myeloid cell-specific *Per1/2* disruption exacerbates diet-induced insulin resistance and glucose intolerance.** Chimeric mice (*BMT-WT* and *BMT-Per1*^{ldc}/*Per2*^{ldc}) were fed an HFD for 12 weeks ($n = 6$–10). *A*, body weight was monitored before and after HFD feeding. *B*, food intake was recorded during the feeding period and calculated as food consumption (*g*) per day per mouse. *Right panel*, feeding efficiency was calculated as the ratio of food intake to body weight. *C*, plasma levels of insulin. *D*, plasma levels of glucose. *E*, insulin tolerance tests. *F*, glucose tolerance tests. For *A–F*, data are the means ± S.E. *, $p < 0.05$; **, $p < 0.01$ BMT-*Per1*^{ldc}/*Per2*^{ldc} *versus* BMT-WT (*B–D*) under the same conditions (*A*) or time points (*E* and *F*). For *C–F*, HFD-fed chimeric mice were fasted for 4 h starting at the same time of the day before tissue collection or physiological assays. For *E* and *F*, mice were given a peritoneal injection of insulin (1 unit/kg) (*E*) or glucose (2 g/kg) (*F*).

BMT-WT mice. After HFD feeding, BMT-*Per1*^{ldc}/*Per2*^{ldc} mice gained more body weight and consumed more food than BMT-WT mice (Fig. 9, *A* and *B*). However, feeding efficiency did not differ between two groups of chimeric mice (Fig. 9*B*). Compared with HFD-fed BMT-WT mice, HFD-fed BMT-*Per1*^{ldc}/*Per2*^{ldc} mice exhibited a significant increase in plasma insulin and glucose levels (Fig. 9, *C* and *D*); however, plasma triglyceride and free fatty acid levels remained unchanged (data not shown). In addition, HFD-fed BMT-*Per1*^{ldc}/*Per2*^{ldc} mice displayed a significant increase in the severity of insulin resistance and glucose intolerance indicated by insulin and glucose tolerance testes, respectively (Fig. 9, *E* and *F*). Thus, disruption of myeloid cell-specific circadian clock mechanism is sufficient to exacerbate HFD-induced insulin resistance and metabolic dysregulation.

Myeloid Cell-specific Per1/2 Disruption Exacerbates Liver Inflammatory Responses, Insulin Resistance, and Metabolic Dysregulation—During obesity, adipose tissue inflammation and dysfunction can produce distal effects on liver inflammatory and metabolic responses (43, 48), which in turn also contribute to the control of systemic insulin sensitivity and glucose homeostasis. Thus, we used the same BMT-WT and BMT-*Per1*^{ldc}/*Per2*^{ldc} mice to concurrently analyze the effect of myeloid cell-specific circadian clock disruption on liver responses. Compared with HFD-fed BMT-WT mice, HFD-fed BMT-*Per1*^{ldc}/*Per2*^{ldc} mice exhibited a significant increase in liver inflammatory responses, indicated by the increases in the phosphorylation of JNK1 (1.7-fold) and NF-κB p65 (2-fold) (Fig. 10*A*) and in the mRNA levels of IL-1β, IL-6, and TNFα (Fig. 10*B*). Meanwhile, HFD-fed BMT-*Per1*^{ldc}/*Per2*^{ldc} mice displayed a significant increase in liver weight (Fig. 10*C*) and a corresponding increase in the severity of hepatic steatosis (Fig. 10*D*). When insulin signaling was analyzed, liver tissue from HFD-fed BMT-*Per1*^{ldc}/*Per2*^{ldc} mice showed significant decreases in insulin-induced Akt phosphorylation (Ser-473) (Fig. 10*E*). Consistent with increased severity of hepatic steatosis, HFD-fed BMT-*Per1*^{ldc}/*Per2*^{ldc} mice were distinguished from controls by a significant increase in liver mRNA levels of SREBP1c and FAS, which are, respectively, a critical transcription factor and a lipogenic enzyme that promotes lipogenesis and hepatic steatosis (Fig. 10*F*) relative to that found in control mice. These results indicate that similar to adipose tissue, HFD-induced liver metabolic dysregulation is amplified by myeloid cell-specific *Per1/2* disruption.

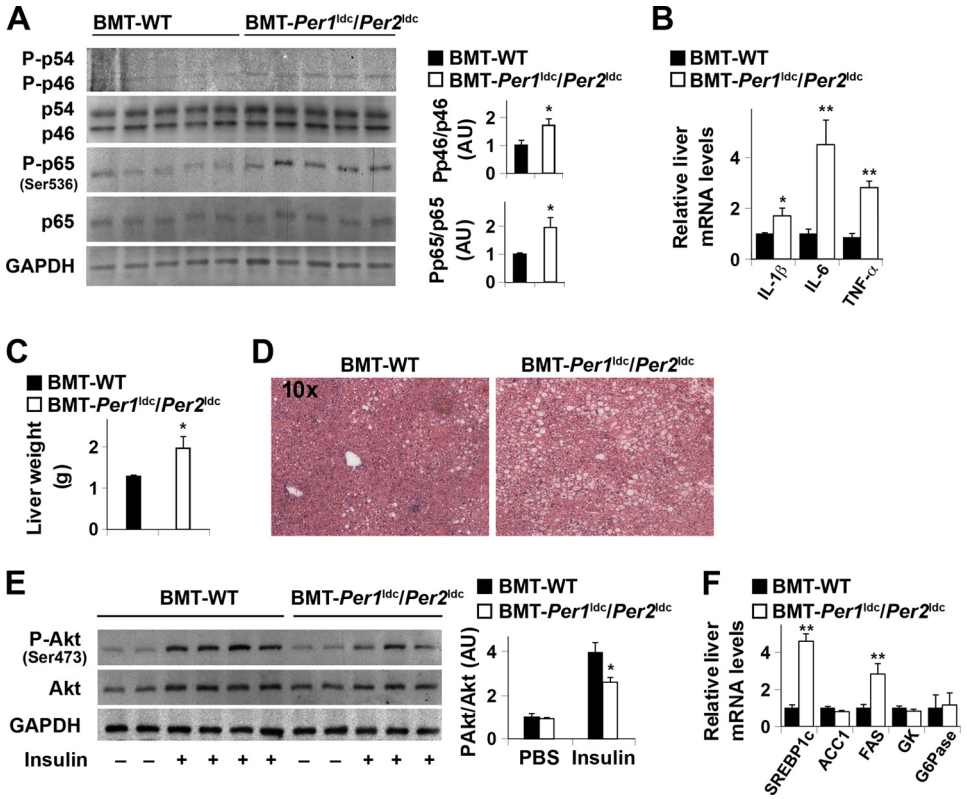

FIGURE 10. **Myeloid cell-specific *Per1/2* disruption exacerbates HFD-induced liver inflammatory responses and insulin resistance.** Chimeric mice (BMT-WT and BMT-*Per1*^{ldc}/*Per2*^{ldc}) were fed an HFD for 12 weeks ($n = 6–10$). *A*, liver inflammatory signaling. The levels of total and phosphorylated JNK1 (p46) and NF-κB p65 were examined using Western blot analyses and quantified using densitometry. *B*, liver levels of proinflammatory cytokine mRNAs. *C*, liver weight. *D*, liver histology (H&E staining). *E*, liver insulin signaling. *F*, liver mRNA levels of key metabolic genes. For *A–F*, HFD-fed chimeric mice were fasted for 4 h starting at the same time of the day before tissue collection (*A–D* and *F*) or insulin injection (*E*). For *B* and *F*, liver mRNA levels of metabolic genes were quantified using real-time PCR and plotted as relative expression. For *E*, chimeric mice were given a bolus injection of insulin (1 unit/kg of body weight) or PBS into the portal vein. For *bar graphs* (*A–C*, *E*, and *F*), data are the means ± S.E. *, $p < 0.05$; **, $p < 0.01$ BMT-*Per1*^{ldc}/*Per2*^{ldc} *versus* BMT-WT (*A–C*) under same condition (insulin in *E*) for the same gene (*F*). *AU*, arbitrary units. *GK*, glucokinase; *ACC1*, acetyl-CoA carboxylase 1; *G6Pase*, glucose-6-phosphatase.

DISCUSSION

During obesity, macrophage proinflammatory activation initiates or aggravates inflammation in key metabolic organs including adipose and liver tissues, thereby leading to systemic insulin resistance. However, it remains to be elucidated exactly how over-nutrition induces proinflammatory activation of macrophages, particularly in those found in adipose tissue where increased inflammation plays a causal role in the pathogenesis of insulin resistance (4–8). In parallel with this inductive effect on macrophage proinflammatory activation (5), HFD feeding has been shown to decrease the amplitude of adipose tissue clock gene rhythms in *Bmal1*, *Clock*, and *Per 2* expression (34) and to lengthen the period of the *Per2* rhythm in cultured adipose tissue (49). Taken together, these observations suggest that dysregulation of peripheral circadian clocks may link diet-associated obesity to adipose tissue inflammation. In support of this putative association, the present study demonstrates that in HFD-fed mice where minor increases in period of the activity of rhythm were similar to those observed previously (34), over-nutrition caused dysregulation of peripheral circadian clocks (*i.e.* substantial increases in the period of *Per 2* oscillations) specifically within key mediators of adipose tissue inflammation, macrophages in stromal vascular cells, and BMDM. Furthermore, the diet-related clock dysregulation in BMDM was accompanied by increased proinflammatory activation. It is noteworthy that our findings provide evidence for the direct link between circadian clock dysregulation and macrophage proinflammatory activation in diet-induced obesity. Specifically, clock-disrupted (*Per1*^{ldc}/*Per2*^{ldc}) macrophages are distinguished by enhanced proinflammatory activation, and myeloid cell-specific clock disruption (*Per1*^{ldc}/*Per2*^{ldc}) exacerbates diet-induced inflammation and insulin resistance in chimeric mice repopulated with only mutant bone marrow cells. As such, the current study indicates for the first time that dysregulation of the macrophage circadian clock (*e.g. Per1/2* disruption) is a critical factor in the mechanism through which over-nutrition induces macrophage proinflammatory activation, thereby leading to adipose tissue inflammation in the context of systemic insulin resistance and hyperglycemia.

Per1 and *Per2* are vital components of the circadian clock mechanism and function as negative regulators in feedback loops involving interactions between *Bmal1*, *Clock*, and the cryptochrome (*Cry1* and *Cry2*) genes (50). Previously, genetic or environmental disruption of circadian clock function has been shown to alter macrophage proinflammatory responses. In macrophages, conditional targeting of Bmal1 abolishes the rhythmic gating of innate immune responses such that cytokine responsiveness to LPS stimulation remains constantly elevated (33). Environmental disruption of circadian rhythms after weekly 6-h shifts in the light-dark cycle similarly exacerbates

inflammatory responses of peritoneal macrophages to LPS challenge in the absence of sleep loss or stress effects (35). In the present analysis of *Per1*^{ldc}/*Per2*^{ldc} mice that are characterized by a globally arrhythmic phenotype (37), circadian clock dysfunction did not influence macrophage differentiation, as the percentage of mature macrophages (F4/80$^+$ CD11b$^+$ cells) differentiated from bone marrow cells of *Per1*^{ldc}/*Per2*^{ldc} mice was identical to that found in wild-type mice. However, among mature macrophages, *Per1*/*2*-disrupted cells showed a much higher percentage of CD11c$^+$ CD206$^-$ cells, indicating increased macrophage proinflammatory activation. The macrophage inflammatory status was corroborated by the finding that *Per1*/*2* disruption increased JNK1 and NF-κB p65 phosphorylation and IL-1β and TNFα expression in mature macrophages under LPS-stimulated conditions. Thus, *Per1*/*2* disruption-associated circadian dysfunction increases macrophage proinflammatory activation.

How the *Per1* and *Per2* genes regulate macrophage activation remains to be determined. It is possible that *Per1* and *Per2* modify inflammatory gene expression through their feedback regulation of CLOCK/BMAL1 transcriptional activity. Indeed, CLOCK has been shown to function as a positive regulator of the transcription factor NF-κB, which is a critical determinant of inflammatory responses (51). Consequently, the relative increases in CLOCK levels observed in peripheral tissues from mutant mice (data not shown) suggest that the loss of negative feedback regulation resulting from *Per1*/*2* disruption may further enhance the activation of NF-κB and ultimately the induction of NF-κB-responsive genes such as IL-1β, TNFα, and other cytokines. Alternatively, *Per1* and *Per2* may alter macrophage inflammatory signaling through interactions with other components of the core or auxiliary feedback loops comprising the molecular clockworks because REV-ERBα has been shown to modulate macrophage TLR signaling (52) and function as an inhibitor of proinflammatory IL-6 release (33). Given that active PPARγ promotes macrophage anti-inflammatory activation (20, 23, 53) and this transcription factor is a molecular target of insulin-sensitizing and anti-diabetic drugs (54), PPARγ may play a role in *Per1*/*2* regulation of macrophage activation. In fact, our data support this hypothesis because PPARγ levels were decreased in *Per1*/*2*-disrupted macrophages in conjunction with their enhanced proinflammatory activation and PPARγ2 overexpression reversed, at least in part, this *Per1*/*2* disruption-associated shift in inflammatory status. Collectively, these observations suggest a novel mechanism for macrophage polarization in which the circadian clock normally acts through PPARγ to inhibit macrophage proinflammatory activation. Because the *PPARγ* promoter contains multiple E-boxes (46), it will be important to determine whether negative feedback by *Per1* and/or *Per2* modulates CLOCK/BMAL1 regulation of E-box mediated transcription of *PPARγ*.

The significance of circadian clock function in macrophage activation was further manifested by the finding that adoptive transfer of *Per1*/*2*-disrupted myeloid cells to wild-type mice exacerbated HFD-induced inflammation and insulin resistance. Notably, BMT-*Per1*^{ldc}/*Per2*^{ldc} mice displayed marked increases in adipose tissue inflammatory responses as indicated by enrichment of mature proinflammatory macrophages in adipose tissue and increased inflammatory signaling and proinflammatory cytokine expression. Consequently, inflammation-associated adipose tissue dysfunction (*i.e.* decreased insulin signaling and adipose tissue metabolic dysregulation) was markedly increased in BMT-*Per1*^{ldc}/*Per2*^{ldc} mice. Given the origin of the myeloid cells/macrophages, the increased severity of adipose tissue inflammatory responses and dysfunction in BMT-*Per1*^{ldc}/*Per2*^{ldc} mice solely reflects proinflammatory activation in clock-disrupted macrophages. This relation was substantiated by the finding that co-culture of adipocytes with *Per1*/*2*-disrupted macrophages increased adipocyte inflammatory response and decreased adipocyte insulin sensitivity. In similar fashion, *Per1*/*2*-disrupted macrophages appeared to mediate the increased severity of liver inflammatory responses and metabolic dysregulation. Altogether, these observations provide convincing evidence that macrophage circadian clock dysregulation is sufficient to potentiate over-nutrition-induced inflammation in adipose tissue and the liver, thereby increasing systemic insulin resistance.

In summary, the present data unveil a novel mechanism for obesity-associated insulin resistance in which circadian clock dysregulation is a key factor that links over-nutrition and macrophage proinflammatory activation to adipose tissue inflammation. At the cellular level, HFD-associated over-nutrition modulates circadian clock function in macrophages, which in turn induces the proinflammatory activation of macrophages, especially those in adipose tissue. When activated, clock-disrupted macrophages are sufficient to exacerbate diet-induced adipose tissue inflammation and systemic insulin resistance. Because adipose tissue inflammatory responses and corresponding insulin sensitivity in over-nutrition-related obesity are differentially engaged by specific types of fatty acids found in HFDs, future studies are warranted to compare the effects of saturated and polyunsaturated fatty acids on macrophage and adipocyte circadian clocks. Thus, it will be important to determine whether saturated fatty acids that activate proinflammatory signaling pathways and lead to impaired insulin sensitivity (*e.g.* palmitate) also modulate the circadian timekeeping function of macrophage and adipocyte clocks and whether this circadian clock dysregulation is blocked or abated by polyunsaturated fatty acids that repress adipose tissue inflammatory responses and have a beneficial impact on insulin sensitivity.

Acknowledgments—We thank P. Hardin and J. Friedman for reviewing the manuscript.

REFERENCES

1. Hossain, P., Kawar, B., and El Nahas, M. (2007) Obesity and diabetes in the developing world: a growing challenge. *N. Engl. J. Med.* **356,** 213–215
2. Angulo, P. (2002) Nonalcoholic fatty liver disease. *N. Engl. J. Med.* **346,** 1221–1231
3. Jensen, M. K., Chiuve, S. E., Rimm, E. B., Dethlefsen, C., Tjønneland, A., Joensen, A. M., and Overvad, K. (2008) Obesity, behavioral lifestyle factors, and risk of acute coronary events. *Circulation* **117,** 3062–3069
4. Weisberg, S. P., McCann, D., Desai, M., Rosenbaum, M., Leibel, R. L., and Ferrante, A. W., Jr. (2003) Obesity is associated with macrophage accumulation in adipose tissue. *J. Clin. Invest.* **112,** 1796–1808
5. Lumeng, C. N., Deyoung, S. M., Bodzin, J. L., and Saltiel, A. R. (2007)

Increased inflammatory properties of adipose tissue macrophages recruited during diet-induced obesity. *Diabetes* **56,** 16–23
6. Kang, K., Reilly, S. M., Karabacak, V., Gangl, M. R., Fitzgerald, K., Hatano, B., and Lee, C.-H. (2008) Adipocyte-derived Th2 cytokines and myeloid PPARδ regulate macrophage polarization and insulin sensitivity. *Cell Metab.* **7,** 485–495
7. Huo, Y., Guo, X., Li, H., Wang, H., Zhang, W., Wang, Y., Zhou, H., Gao, Z., Telang, S., Chesney, J., Chen, Y. E., Ye, J., Chapkin, R. S., and Wu, C. (2010) Disruption of inducible 6-phosphofructo-2-kinase ameliorates diet-induced adiposity but exacerbates systemic insulin resistance and adipose tissue inflammatory response. *J. Biol. Chem.* **285,** 3713–3721
8. Guo, X., Xu, K., Zhang, J., Li, H., Zhang, W., Wang, H., Lange, A. J., Chen, Y. E., Huo, Y., and Wu, C. (2010) Involvement of inducible 6-phosphofructo-2-kinase in the anti-diabetic effect of PPARγ activation in mice. *J. Biol. Chem.* **285,** 23711–23720
9. Qatanani, M., and Lazar, M. A. (2007) Mechanisms of obesity-associated insulin resistance: many choices on the menu. *Genes Dev.* **21,** 1443–1455
10. Kahn, B. B., and Flier, J. S. (2000) Obesity and insulin resistance. *J. Clin. Invest.* **106,** 473–481
11. Rosen, E. D., and Spiegelman, B. M. (2006) Adipocytes as regulators of energy balance and glucose homeostasis. *Nature* **444,** 847–853
12. Badman, M. K., and Flier, J. S. (2007) The adipocyte as an active participant in energy balance and metabolism. *Gastroenterology* **132,** 2103–2115
13. Hotamisligil, G. S., Peraldi, P., Budavari, A., Ellis, R., White, M. F., and Spiegelman, B. M. (1996) IRS-1-mediated inhibition of insulin receptor tyrosine kinase activity in TNF-α- and obesity-induced insulin resistance. *Science* **271,** 665–668
14. Cheung, A. T., Ree, D., Kolls, J. K., Fuselier, J., Coy, D. H., and Bryer-Ash, M. (1998) An *in vivo* model for elucidation of the mechanism of tumor necrosis factor-α (TNF-α)-induced insulin resistance: evidence for differential regulation of insulin signaling by TNF-α. *Endocrinology* **139,** 4928–4935
15. Cheung, A. T., Wang, J., Ree, D., Kolls, J. K., and Bryer-Ash, M. (2000) Tumor necrosis factor-α induces hepatic insulin resistance in obese Zucker (fa/fa) rats via interaction of leukocyte antigen-related tyrosine phosphatase with focal adhesion kinase. *Diabetes* **49,** 810–819
16. Boden, G., Cheung, P., Stein, T. P., Kresge, K., and Mozzoli, M. (2002) FFA cause hepatic insulin resistance by inhibiting insulin suppression of glycogenolysis. *Am. J. Physiol. Endocrinol. Metab.* **283,** E12–E19
17. Berg, A. H., Combs, T. P., Du, X., Brownlee, M., and Scherer, P. E. (2001) The adipocyte-secreted protein Acrp30 enhances hepatic insulin action. *Nat. Med.* **7,** 947–953
18. Kabir, M., Catalano, K. J., Ananthnarayan, S., Kim, S. P., Van Citters, G. W., Dea, M. K., and Bergman, R. N. (2005) Molecular evidence supporting the portal theory: a causative link between visceral adiposity and hepatic insulin resistance. *Am. J. Physiol. Endocrinol. Metab.* **288,** E454–E461
19. Xu, H., Barnes, G. T., Yang, Q., Tan, G., Yang, D., Chou, C. J., Sole, J., Nichols, A., Ross, J. S., Tartaglia, L. A., and Chen, H. (2003) Chronic inflammation in fat plays a crucial role in the development of obesity-related insulin resistance. *J. Clin. Invest.* **112,** 1821–1830
20. Stienstra, R., Duval, C., Keshtkar, S., van der Laak, J., Kersten, S., and Müller, M. (2008) Peroxisome proliferator-activated receptor γ activation promotes infiltration of alternatively activated macrophages into adipose tissue. *J. Biol. Chem.* **283,** 22620–22627
21. Todoric, J., Löffler, M., Huber, J., Bilban, M., Reimers, M., Kadl, A., Zeyda, M., Waldhäusl, W., and Stulnig, T. (2006) Adipose tissue inflammation induced by high-fat diet in obese diabetic mice is prevented by n-3 polyunsaturated fatty acids. *Diabetologia* **49,** 2109–2119
22. Lumeng, C. N., Bodzin, J. L., and Saltiel, A. R. (2007) Obesity induces a phenotypic switch in adipose tissue macrophage polarization. *J. Clin. Invest.* **117,** 175–184
23. Odegaard, J. I., Ricardo-Gonzalez, R. R., Goforth, M. H., Morel, C. R., Subramanian, V., Mukundan, L., Red Eagle, A., Vats, D., Brombacher, F., Ferrante, A. W., and Chawla, A. (2007) Macrophage-specific PPARγ controls alternative activation and improves insulin resistance. *Nature* **447,** 1116–1120
24. Odegaard, J. I., Ricardo-Gonzalez, R. R., Red Eagle, A., Vats, D., Morel, C. R., Goforth, M. H., Subramanian, V., Mukundan, L., Ferrante, A. W., and Chawla, A. (2008) Alternative M2 activation of Kupffer cells by PPARd ameliorates obesity-induced insulin resistance. *Cell Metab.* **7,** 496–507
25. Sag, D., Carling, D., Stout, R. D., and Suttles, J. (2008) Adenosine 5′-monophosphate-activated protein kinase promotes macrophage polarization to an anti-inflammatory functional phenotype. *J. Immunol.* **181,** 8633–8641
26. Saberi, M., Woods, N.-B., de Luca, C., Schenk, S., Lu, J. C., Bandyopadhyay, G., Verma, I. M., and Olefsky, J. M. (2009) Hematopoietic cell-specific deletion of toll-like receptor 4 ameliorates hepatic and adipose tissue insulin resistance in high-fat-fed mice. *Cell Metab.* **10,** 419–429
27. Solinas, G., Vilcu, C., Neels, J. G., Bandyopadhyay, G. K., Luo, J.-L., Naugler, W., Grivennikov, S., Wynshaw-Boris, A., Scadeng, M., Olefsky, J. M., and Karin, M. (2007) JNK1 in hematopoietically derived cells contributes to diet-induced inflammation and insulin resistance without affecting obesity. *Cell Metab.* **6,** 386–397
28. Han, M. S., Jung, D. Y., Morel, C., Lakhani, S. A., Kim, J. K., Flavell, R. A., and Davis, R. J. (2013) JNK expression by macrophages promotes obesity-induced insulin resistance and inflammation. *Science* **339,** 218–222
29. Turek, F. W., Joshu, C., Kohsaka, A., Lin, E., Ivanova, G., McDearmon, E., Laposky, A., Losee-Olson, S., Easton, A., Jensen, D. R., Eckel, R. H., Takahashi, J. S., and Bass, J. (2005) Obesity and metabolic syndrome in circadian Clock mutant mice. *Science* **308,** 1043–1045
30. Marcheva, B., Ramsey, K. M., Buhr, E. D., Kobayashi, Y., Su, H., Ko, C. H., Ivanova, G., Omura, C., Mo, S., Vitaterna, M. H., Lopez, J. P., Philipson, L. H., Bradfield, C. A., Crosby, S. D., JeBailey, L., Wang, X., Takahashi, J. S., and Bass, J. (2010) Disruption of the clock components CLOCK and BMAL1 leads to hypoinsulinaemia and diabetes. *Nature* **466,** 627–631
31. Paschos, G. K., Ibrahim, S., Song, W.-L., Kunieda, T., Grant, G., Reyes, T. M., Bradfield, C. A., Vaughan, C. H., Eiden, M., Masoodi, M., Griffin, J. L., Wang, F., Lawson, J. A., and Fitzgerald, G. A. (2012) Obesity in mice with adipocyte-specific deletion of clock component Arntl. *Nat. Med.* **18,** 1768–1777
32. Keller, M., Mazuch, J., Abraham, U., Eom, G. D., Herzog, E. D., Volk, H.-D., Kramer, A., and Maier, B. (2009) A circadian clock in macrophages controls inflammatory immune responses. *Proc. Natl. Acad. Sci. U.S.A.* **106,** 21407–21412
33. Gibbs, J. E., Blaikley, J., Beesley, S., Matthews, L., Simpson, K. D., Boyce, S. H., Farrow, S. N., Else, K. J., Singh, D., Ray, D. W., and Loudon, A. S. (2012) The nuclear receptor REV-ERBa mediates circadian regulation of innate immunity through selective regulation of inflammatory cytokines. *Proc. Natl. Acad. Sci. U.S.A.* **109,** 582–587
34. Kohsaka, A., Laposky, A. D., Ramsey, K. M., Estrada, C., Joshu, C., Kobayashi, Y., Turek, F. W., and Bass, J. (2007) High-fat diet disrupts behavioral and molecular circadian rhythms in mice. *Cell Metab.* **6,** 414–421
35. Castanon-Cervantes, O., Wu, M., Ehlen, J. C., Paul, K., Gamble, K. L., Johnson, R. L., Besing, R. C., Menaker, M., Gewirtz, A. T., and Davidson, A. J. (2010) Dysregulation of inflammatory responses by chronic circadian disruption. *J. Immunol.* **185,** 5796–5805
36. Yoo, S.-H., Yamazaki, S., Lowrey, P. L., Shimomura, K., Ko, C. H., Buhr, E. D., Siepka, S. M., Hong, H.-K., Oh, W. J., Yoo, O. J., Menaker, M., and Takahashi, J. S. (2004) PERIOD2::LUCIFERASE real-time reporting of circadian dynamics reveals persistent circadian oscillations in mouse peripheral tissues. *Proc. Natl. Acad. Sci. U.S.A.* **101,** 5339–5346
37. Bae, K., Jin, X., Maywood, E. S., Hastings, M. H., Reppert, S. M., and Weaver, D. R. (2001) Differential functions of mPer1, mPer2, and mPer3 in the SCN circadian clock. *Neuron* **30,** 525–536
38. Wu, C., Okar, D. A., Newgard, C. B., and Lange, A. J. (2001) Overexpression of 6-phosphofructo-2-kinase/fructose-2,6-bisphosphatase in mouse liver lowers blood glucose by suppression of hepatic glucose production. *J. Clin. Invest.* **107,** 91–98
39. Wu, C., Kang, J. E., Peng, L. J., Li, H., Khan, S. A., Hillard, C. J., Okar, D. A., and Lange, A. J. (2005) Enhancing hepatic glycolysis reduces obesity: differential effects on lipogenesis depend on site of glycolytic modulation. *Cell Metab.* **2,** 131–140
40. Ko, M. L., Shi, L., Tsai, J.-Y., Young, M. E., Neuendorff, N., Earnest, D. J., and Ko, G. Y. (2011) Cardiac-specific mutation of Clock alters the quan-

titative measurements of physical activities without changing behavioral circadian rhythms. *J. Biol. Rhythms* **26,** 412–422
41. Farnell, Y. F., Shende, V. R., Neuendorff, N., Allen, G. C., and Earnest, D. J. (2011) Immortalized cell lines for real-time analysis of circadian pacemaker and peripheral oscillator properties. *Eur. J. Neurosci.* **33,** 1533–1540
42. Prieur, X., Mok, C. Y., Velagapudi, V. R., Núñez, V., Fuentes, L., Montaner, D., Ishikawa, K., Camacho, A., Barbarroja, N., O'Rahilly, S., Sethi, J. K., Dopazo, J., Orešič, M., Ricote, M., and Vidal-Puig, A. (2011) Differential lipid partitioning between adipocytes and tissue macrophages modulates macrophage lipotoxicity and M2/M1 polarization in obese mice. *Diabetes* **60,** 797–809
43. Huo, Y., Guo, X., Li, H., Xu, H., Halim, V., Zhang, W., Wang, H., Fan, Y.-Y., Ong, K. T., Woo, S.-L., Chapkin, R. S., Mashek, D. G., Chen, Y., Dong, H., Lu, F., Wei, L., and Wu, C. (2012) Targeted overexpression of inducible 6-phosphofructo-2-kinase in adipose tissue increases fat deposition but protects against diet-induced insulin resistance and inflammatory responses. *J. Biol. Chem.* **287,** 21492–21500
44. Guo, X., Li, H., Xu, H., Halim, V., Thomas, L. N., Woo, S.-L., Huo, Y., Chen, Y. E., Sturino, J. M., and Wu, C. (2013) Disruption of inducible 6-phosphofructo-2-kinase impairs the suppressive effect of PPARγ activation on diet-induced intestine inflammatory response. *J. Nutr. Biochem.* **24,** 770–775
45. Guo, X., Li, H., Xu, H., Halim, V., Zhang, W., Wang, H., Ong, K. T., Woo, S. L., Walzem, R. L., Mashek, D. G., Dong, H., Lu, F., Wei, L., Huo, Y., and Wu, C. (2012) Palmitoleate induces hepatic steatosis but suppresses liver inflammatory response in mice. *PLoS ONE* **7,** e39286
46. Herzig, S., Hedrick, S., Morantte, I., Koo, S. H., Galimi, F., and Montminy, M. (2003) CREB controls hepatic lipid metabolism through nuclear hormone receptor PPAR-γ. *Nature* **426,** 190–193
47. Zhang, J., Fu, M., Cui, T., Xiong, C., Xu, K., Zhong, W., Xiao, Y., Floyd, D., Liang, J., Li, E., Song, Q., and Chen, Y. E. (2004) Selective disruption of PPARγ2 impairs the development of adipose tissue and insulin sensitivity. *Proc. Natl. Acad. Sci. U.S.A.* **101,** 10703–10708
48. Kamei, N., Tobe, K., Suzuki, R., Ohsugi, M., Watanabe, T., Kubota, N., Ohtsuka-Kowatari, N., Kumagai, K., Sakamoto, K., Kobayashi, M., Yamauchi, T., Ueki, K., Oishi, Y., Nishimura, S., Manabe, I., Hashimoto, H., Ohnishi, Y., Ogata, H., Tokuyama, K., Tsunoda, M., Ide, T., Murakami, K., Nagai, R., and Kadowaki, T. (2006) Overexpression of monocyte chemoattractant protein-1 in adipose tissues causes macrophage recruitment and insulin resistance. *J. Biol. Chem.* **281,** 26602–26614
49. Shi, S.-Q., Ansari, T. S., McGuinness, O. P., Wasserman, D. H., and Johnson, C. H. (2013) Circadian disruption leads to insulin resistance and obesity. *Curr. Biol.* **23,** 372–381
50. Bass, J., and Takahashi, J. S. (2010) Circadian integration of metabolism and energetics. *Science* **330,** 1349–1354
51. Spengler, M. L., Kuropatwinski, K. K., Comas, M., Gasparian, A. V., Fedtsova, N., Gleiberman, A. S., Gitlin, I. I., Artemicheva, N. M., Deluca, K. A., Gudkov, A. V., and Antoch, M. P. (2012) Core circadian protein CLOCK is a positive regulator of NF-kB-mediated transcription. *Proc. Natl. Acad. Sci. U.S.A.* **109,** E2457–E2465
52. Fontaine, C., Rigamonti, E., Pourcet, B., Duez, H., Duhem, C., Fruchart, J.-C., Chinetti-Gbaguidi, G., and Staels, B. (2008) The nuclear receptor Rev-erba is a liver X receptor (LXR) target gene driving a negative feedback loop on select LXR-induced pathways in human macrophages. *Mol. Endocrinol.* **22,** 1797–1811
53. Bouhlel, M. A., Derudas, B., Rigamonti, E., Dièvart, R., Brozek, J., Haulon, S., Zawadzki, C., Jude, B., Torpier, G., Marx, N., Staels, B., and Chinetti-Gbaguidi, G. (2007) PPARγ activation primes human monocytes into alternative M2 macrophages with anti-inflammatory properties. *Cell Metab.* **6,** 137–143
54. Hevener, A. L., Olefsky, J. M., Reichart, D., Nguyen, M. T., Bandyopadyhay, G., Leung, H. Y., Watt, M. J., Benner, C., Febbraio, M. A., Nguyen, A. K., Folian, B., Subramaniam, S., Gonzalez, F. J., Glass, C. K., and Ricote, M. (2007) Macrophage PPARγ is required for normal skeletal muscle and hepatic insulin sensitivity and full antidiabetic effects of thiazolidinediones. *J. Clin. Invest.* **117,** 1658–1669